GEOMETRY AND COMPOSITION OF ICE BANKS IN A MACROTIDAL CHANNEL

by

CarolAnne Black

Submitted in partial fulfillment of the requirements
for the degree of Master of Science

at

Dalhousie University
Halifax, Nova Scotia
May 2013

DALHOUSIE UNIVERSITY

DEPARTMENT OF OCEANOGRAPHY

The undersigned hereby certify that they have read and recommend to the Faculty of Graduate Studies for acceptance a thesis entitled "GEOMETRY AND COMPOSITION OF ICE BANKS IN A MACROTIDAL CHANNEL" by CarolAnne Black in partial fulfillment of the requirements for the degree of Master of Science.

Dated: May 17, 2013

External Examiner: _____
Dr. Brian G. Sanderson

Supervisor: _____
Dr. Paul S. Hill

Readers: _____
Dr. Alex E. Hay

_____
Dr. Tetjana Ross

DALHOUSIE UNIVERSITY

DATE: May 17, 2013

AUTHOR: CarolAnne Black

TITLE: GEOMETRY AND COMPOSITION OF ICE BANKS IN A MACROTIDAL CHANNEL

DEPARTMENT OR SCHOOL: Department of Oceanography

DEGREE: M.Sc. CONVOCATION: October YEAR: 2013

_____

Signature of Author

For my Dad, who would be so proud;
and for my Mom, who is.

TABLE OF CONTENTS

List of Tables . . . . . **viii**

List of Figures . . . . . **ix**

Abstract . . . . . **xi**

List of Abbreviations and Symbols Used . . . . . **xii**

Glossary of terms . . . . . **xiv**

0.1 frazil ice xiv

0.2 grease ice xiv

0.3 pan ice xiv

0.4 floe ice xiv

0.5 cake ice xiv

0.6 composite ice xv

0.7 drift ice xv

0.8 stranded ice xv

0.9 shorefast ice xv

0.10 ice field xv

0.11 ice wall xvi

Acknowledgements . . . . . **xvii**

Chapter 1 Introduction **1**

Chapter 2 Ice formation in macrotidal estuaries **5**

2.1 Introduction to study sites 7

2.2 Ice formation - initial stages 7

2.3 Stranding and the initial stages of ice block formation 9

2.4 Ice fields 11

2.5 Ice wall formation in narrow tidal channels 14

2.6 Formation of large ice blocks . . . 17
2.7 Mechanisms that increase the sediment to ice ratio in ice blocks . . . 18
2.8 Hypotheses . . . 20
2.8.1 Conceptual Model Introduction . . . 20
2.8.2 Model 1: Modified Bank Materials . . . 22
2.8.3 Model 2: Modified Friction . . . 23
2.9 Summary and Objectives . . . 24

Chapter 3 Methods . . . 25
3.1 Channel morphology . . . 25
3.1.1 Uncertainties . . . 27
3.2 Sediment . . . 28
3.2.1 Uncertainties . . . 28
3.3 Ice . . . 29
3.3.1 Ice block samples . . . 30
3.3.2 Ice cores . . . 32
3.3.3 Uncertainties . . . 33
3.4 Environmental measurements . . . 34
3.4.1 Uncertainties . . . 34

Chapter 4 Results . . . 37
4.1 Channel morphology . . . 37
4.2 Sediment . . . 38
4.3 Ice . . . 39
4.3.1 Ice block samples . . . 39
4.3.2 Ice cores . . . 41
4.4 Environmental measurements . . . 42

Chapter 5 Discussion . . . 45
5.1 Why do ice walls form? . . . 45
5.1.1 Fractional increase in drag coefficient . . . 47
5.2 Environmental conditions that lead to ice walls and their collapse . . . 50
5.2.1 Was 2012 a typical year? . . . 51
5.3 Negatively buoyant ice . . . 53

5.4 Do negatively buoyant ice blocks pose a threat? 57

Chapter 6 Conclusions **58**

6.1 Conclusions 58

6.2 Future research 59

Appendix A **60**

Bibliography **62**

List of Tables

3.1 Dates of visits to the Kennetcook River site over the 2011 to 2012 field season 26

3.2 Three sieve replicates 30

3.3 Ice block samples collected in 2011 30

3.4 Ice block samples collected in 2012 30

3.5 Ice core samples collected in 2012 32

4.1 Ice block densities from 13 samples collected in Winter 2011 41

4.2 Ice block densities from 4 samples collected in Winter 2012 41

4.3 Maximum ice core densities from 12 samples collected on the north side ice wall at the Kennetcook River bridge in Winter 2012 42

5.1 Cumulative negative degree hours from January to March for the 5 years preceding 2012 52

5.2 Estimates of timing of ice wall formation and collapse in previous years 52

5.3 Summary of sediment mass percentages in samples from previous studies 56

A.1 Kennetcook River depth at 41 positions across the channel width from October 19, 2011 to May 8, 2012 60

LIST OF FIGURES

1.1	Map of the Minas Basin, Bay of Fundy	2
1.2	Sediment-laden ice block, stranded at Debert Beach	3
2.1	Diagram showing the life cycle of the Minas Basin ice	6
2.2	Grease, pan, and floe ice	8
2.3	Stranded, composite and cake ice	10
2.4	Ice fields and their their effects on channel flow	12
2.5	Layering of sediment and ice within ice fields	13
2.6	Diagram of channel profile, showing extent of ice walls	14
2.7	Ice wall formation	15
2.8	The formation of large blocks from ice walls	17
2.9	Examples of plucking	19
2.10	Plucking and differential release	20
2.11	Schematic of effects on channel morphology due to MBM and MF hypotheses	23
3.1	Diagram of bridge and channel for depth measurements	27
3.2	A dried sediment sample	29
3.3	The water displacement apparatus with a sample block that has sunk in the freshwater	31
3.4	Environmental data during study period	35
4.1	Summer and winter profiles of Kennetcook River	38
4.2	Kennetcook River thalweg depth, cross-sectional area, and grain size, over time	39
4.3	Fall profiles of Kennetcook River	40
4.4	Air temperature over study period and relationship to channel cross-sectional area	44
5.1	Stranded ice blocks at the Kennetcook River bridge	46

5.2 Stranded cake ice at Old Barns 47

ABSTRACT

Large ice blocks containing enough sediment to be denser than sea water form in the Minas Basin of the Bay of Fundy. The timing of ice block formation and ice block composition were monitored to improve understanding of the potential threat to tidal power generators posed by collision with ice blocks. Large blocks are produced from ice cliffs that form when anchored ice obstructs tidal channels and decreases flow speed. Decreased flow causes the channel cross-sectional area to decrease. In 2012, the Kennetcook River cross-sectional area decreased by 21% due to the formation of ice cliffs. Large ice blocks separated from the walls during the two spring tides following a 20-day time lag of the minimum air temperature. Ten percent of sampled ice blocks were denser than freshwater. Four of twelve ice cores collected from the ice cliffs along the Kennetcook River contained enough sediment to become denser than seawater.

List of Abbreviations and Symbols Used

Abbreviation	Term
MBM	Modified Bank Materials
MF	Modified Friction

Symbol	Description	Units
$d(y)$	channel depth	m
b	diameter of channel obstructions	m
$d_m(y)$	total measured depth	m
$d_u(y)$	uncertainty in channel depth	m
d_{50}	median grain size	μm
g	acceleration due to gravity	$\mathrm{m\,s^{-2}}$
h	height from high water mark to bridge (north side)	m
h'	sum of channel depth and surface height	m
k	bottom drag coefficient	none
k_{app}	obstruction drag coefficient	none
k_b	bed drag coefficient	none
$u(t)$	depth-integrated channel velocity	$\mathrm{m\,s^{-1}}$
t	time	s, hr, d
x	along-channel coordinate	m
y	across-channel coordinate	m
A	channel cross-sectional area	$\mathrm{m^2}$
A_u	uncertainty in cross-sectional area	$\mathrm{m^2}$
C	distance between channel obstructions	m
M_s	sediment mass	kg
M_t	total ice block mass	kg
N	number of measurements	none
Q	discharge	$\mathrm{m^3\,s^{-1}}$

Symbol	Description	Units
T	air temperature	°C
U	velocity	$\mathrm{m\,s^{-1}}$
Y	channel width	m
α	pressure gradient force times depth	$\mathrm{m^2\,s^{-2}}$
ρ	maximum possible ice core density	$\mathrm{kg\,m^{-3}}$
ρ_i	density of freshwater ice	$\mathrm{kg\,m^{-3}}$
ρ_s	density of sediment	$\mathrm{kg\,m^{-3}}$
ρ_w	density of water	$\mathrm{kg\,m^{-3}}$
η	surface height	m
ϕ	bridge slope	radians

GLOSSARY OF TERMS

Below is a glossary of terms used to describe the ice in the Bay of Fundy. Definitions are based on those of *Gordon and Desplanque* (1981), with a few additions.

0.1 frazil ice

Frazil ice is the ice that forms during the first stage of ice block formation. When turbulent water is super-cooled, frazil ice forms as high concentrations of microscopic slivers of ice.

0.2 grease ice

Grease ice is a floating mass of unconsolidated frazil ice crystals and sediment. Grease ice can cover the surface of tidal channels.

0.3 pan ice

Pan ice forms when grease ice consolidates into solid masses. Pieces of pan ice are up to 15 cm thick and up to 50 m in diameter. They are typically circular in shape due to collisions with surrounding ice and have a raised lip around their perimeter.

0.4 floe ice

Floe ice forms when many pieces of pan ice freeze together. Pieces of floe ice are approximately 50 to 100 m in diameter.

0.5 cake ice

Cake ice is ice that is much larger than pan ice and typically has approximately the same height and width. Pieces of cake ice, or cakes, are circular from above due to collisions with surrounding ice and due to erosion by other ice and by passing water. Cakes are large enough to sit on the bed for a significant part of the tidal cycle, if stranded. Stranded

cakes are subjected to increased erosion, which is what causes the large blocks to become cylindrical. The erosion takes place over longer periods of the tidal cycle closer to the base of the block, resulting in a smaller diameter base than top.

0.6 composite ice

Composite ice is made up of a mixture of pieces of ice, frozen together. Composite ice blocks usually form when pieces of ice are rafted on top of stranded or shore-fast ice, or on a smaller scale, when grease ice and pieces of pan ice are rafted on top of one another in open water.

0.7 drift ice

Drift ice is any kind of ice that is moved around the Bay with the tidal currents. Cake ice, composite ice, floe ice, grease ice, and pan ice are all forms of drift ice.

0.8 stranded ice

Stranded ice is ice that is grounded at low tide. Stranded ice is usually re-floated at high tide, but can become shorefast ice if frozen solidly to the substrate.

0.9 shorefast ice

Shorefast ice is ice that has frozen to the substrate and is no longer removed from its location by tidal currents and inundations. It is found on channel banks and bars that are exposed to air during low tide. Ice fields and ice walls are forms of shorefast ice.

0.10 ice field

Ice fields are shorefast ice formations in the wider, shallower parts of the Minas Basin, such as tidal flats and estuaries. They tend to be irregular in shape, made up of all forms of stranded drift ice and tend to incorporate coupled layers of sediment and ice.

0.11 ice wall

Ice walls are shorefast ice formations in the narrower parts of tidal channels, where the channel cross section tends to be rectangular during winter and trapezoidal in other seasons. Ice walls can be up to 5 m in height and can completely cover the channel banks.

ACKNOWLEDGEMENTS

I would like to acknowledge the support of my supervisor, Dr. Paul Hill, my committee members, Dr. Alex Hay and Dr. Tetjana Ross, as well as Dr. Dan Kelley, Laura deGelleke, Dr. Clark Richards, Nick Dourado, and Jackie Hurst. Funding for this project was provided by the Natural Sciences and Engineering Research Council of Canada and by Nova Scotia Power.

To Paul Hill, thank you for being my guide through all of this. To Dan Kelley, you brightened my school days. I loved every one of our un-countable chats. To my partner and the man of my adult life, Tim Scribner. I could've done it without you, but you made it so much more fun. Your "let's do it!" or "that's a crazy idea, but you should go for it anyway," attitude toward absolutely everything makes life wonderful. To Jackie Hurst, thank you for being the best: the best at solving any problem, the best at contagious laughter, the best at smiling. You make the department feel like home. To Clark Richards, thank you for our many chats and all your technical advice, while you were still at Dalhousie, and long after you'd left.

Thank you also to: Laura deGelleke, for your help and pep talks, and for always being able to one-up me when I've told you how I royally screwed something up; Alex Hay and Tetjana Ross, for your ideas and guidance; Nick Dourado, for your help in the field and the lab, and for the piano chats; Daniel, for being almost as good at solving problems, and smiling, as Jackie; Stephanie Kienast, for your help and for reviewing parts of my thesis; Gwen Williams and Janet Stalker, for being such wonderful friends that you agreed to edit parts of this document.

CHAPTER 1

INTRODUCTION

The tidal range in Minas Basin, part of the Bay of Fundy (Figure 1.1), can reach more than 15 m. It is the greatest tidal range in the world. The tides in Minas Basin generate tremendous currents, from which energy may be extracted. In their book on the Bay of Fundy, *Desplanque and Mossman* (2004) put into perspective the quantity of available tidal energy, in relation to traditional hydroelectric power production in rivers: "An average single tidal flow into the Bay of Fundy matches the estimated total daily volume (about 104 km^3) of all the world's river discharges into the oceans".

Bottom-anchored tidal energy generators may be deployed in Minas Basin to extract tidal energy. Such generators may be subjected to threats that could affect their operation. Specifically, large objects in the water column may damage tidal energy generators. *Sanders et al.* (2008) identified three categories of large objects that may be found in the water column near the Minas Passage: dead trees, marine life, and sediment-laden ice blocks. There is a need to quantify the potential risks to bottom-anchored tidal energy generators in the Minas Passage. The goal of this thesis is to increase understanding of the threat posed by sediment-laden ice blocks.

During winter, sediment-laden ice forms in the Minas Basin. *Hind* (1875) was the first to describe it. The concern of Hind's article was the effects of the ice on a canal that was being considered between the Cumberland Basin and the Northumberland Strait. Since then, numerous others have described the ice in relation to tidal energy generation engineering projects, such as tidal barrages (*Sweet*, 1968; *Gordon and Desplanque*, 1981; *Desplanque and Bray*, 1986); in relation to general ice conditions (*Desplanque*, 1967; *Gordon and Desplanque*, 1983); and in relation to sediment transport and dynamics and ecological effects (*Bancroft*, 1905; *Knight and Dalrymple*, 1976; *Gordon and Desplanque*,

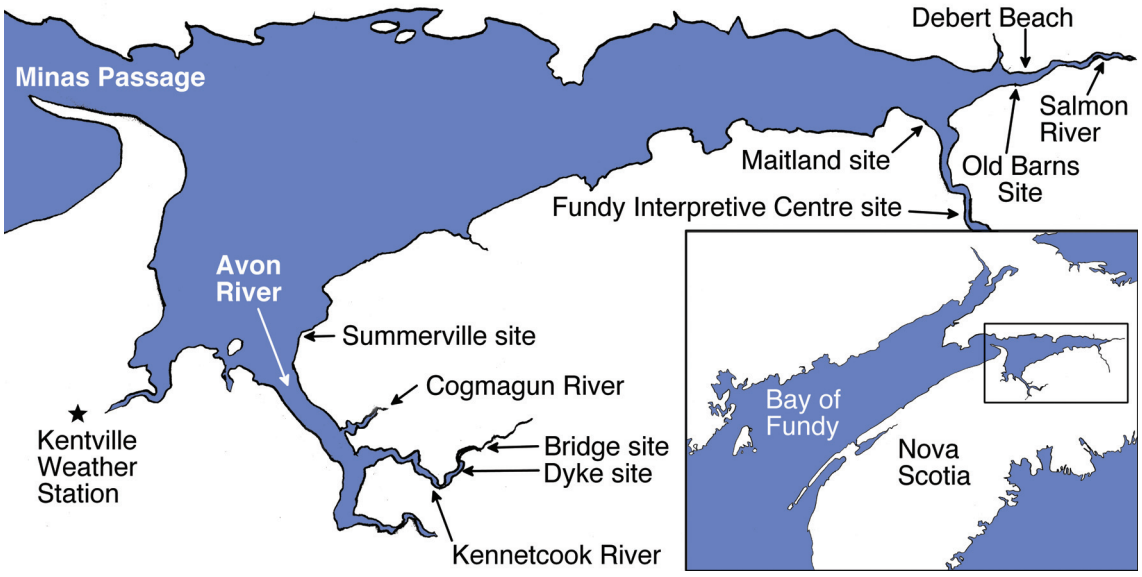

Figure 1.1: Map of the Minas Basin, Bay of Fundy. Field sites are indicated for Summerville; the Kennetcook River Bridge and Dyke; Maitland and Fundy Interpretive Centre, along the Shubenacadie River; and Debert Beach and Old Barns, along the Salmon River. The inset is of the greater Bay of Fundy region and indicated within it is the location of the Minas Basin. The location of the Kentville weather station is also indicated.

1981, 1983; *Ollerhead et al.*, 1999; *vanProosdij et al.*, 2006). A number of these studies involved analyses of the sediment content of ice blocks (*Hind*, 1875; *Sweet*, 1968; *Knight and Dalrymple*, 1976; *Ollerhead et al.*, 1999; *Sanders et al.*, 2008). However, only more recently has the possibility of neutrally, or negatively, buoyant ice been examined in the literature (*Sanders and Baddour*, 2006; *Sanders et al.*, 2008; *Sanders*, 2011).

The anomalous combination of conditions in the Bay of Fundy - cold temperatures, macrotides, and high water column sediment content - present the opportunity for the formation of large blocks of sediment-laden ice. Their volume may exceed fifty cubic meters (Figure 1.2). Blocks have been found to accumulate sediment and may become neutrally or negatively buoyant.

Negatively buoyant sediment-laden ice was first reported by *Gordon and Desplanque* (1981), who describe their observations of the characteristics and dynamics of ice blocks found on the mudflats in Cumberland Basin. The authors noted that “some pieces of drift ice, heavily-laden with sediment (perhaps derived from fractured shorefast ice) roll along the bottom”. They also describe observing neutrally buoyant ice and gouges in mudflats

at low tide after the passing of the blocks. The negatively buoyant fraction of ice blocks was first determined by *Sanders et al.* (2008). Of ten ice block samples, collected from the intertidal mudflats in the Bay of Fundy, *Sanders et al.* (2008) found that three had a negative probable buoyancy.

Large neutrally or negatively buoyant ice blocks, formed in Minas Basin, could migrate with the ebb tide into the Minas Passage and collide with bottom-anchored tidal energy generators. The formation, density, quantity, and fate of these ice blocks are all of interest in characterizing the risk to bottom-anchored tidal energy generators.

Figure 1.2: Co-op student Robbie Paterson with a sediment-laden ice block at Debert Beach. Of a scattering of blocks on the beach on February 24, 2011, this was one of the largest.

Much previous observational evidence exists for how sediment-laden ice blocks form and behave, as described in detail in Chapter 2. A gap in knowledge still exists, however, in the understanding of the mechanisms of formation and characterization of the ice blocks. The aim of this Masters project is to increase the understanding of the composition and

of the processes of formation of large, sediment-laden ice blocks. This thesis addresses questions related to how ice blocks form in Minas Basin and what fraction of them may have densities that make them neutrally or negatively buoyant. This work is part of a larger project addressing numerous aspects of the threat sediment-laden ice blocks pose to tidal turbines.

CHAPTER 2

ICE FORMATION IN MACROTIDAL ESTUARIES

At the onset of below-freezing temperatures, the morphology of the channels connected to the Minas Basin changes. Over time scales of days to weeks, ice takes over the banks and ice walls up to 5 m high can form (*Desplanque and Mossman*, 2004). The new morphology lasts until the end of winter (*Knight and Dalrymple*, 1976). Large sediment-laden ice blocks form when channel ice walls collapse (*Sanders et al.*, 2008). (For a diagram of the life cycle of Minas Basin ice, see Figure 2.1.)

This chapter includes a qualitative description of how sediment-laden ice forms in macrotidal estuaries in the Minas Basin, as well as a description of this project's central hypotheses. Two end-member hypotheses were developed to help explain the change in morphology that takes place in Minas Basin tidal channels over the winter. These simple models, plus observations of channel morphology and sediment texture, are used to examine hydraulic changes in channels in winter.

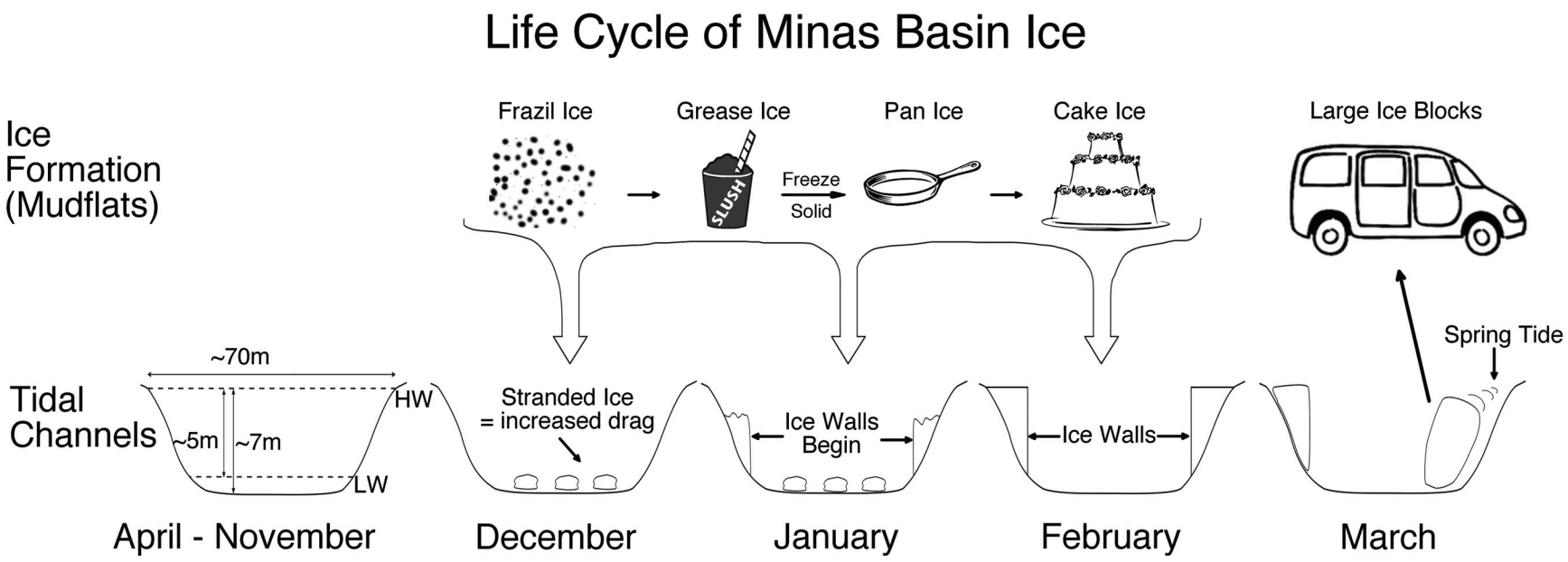

Figure 2.1: Diagram showing the life cycle of Minas Basin ice. Frazil ice, represented by a mass of tiny dots, is the microscopic slivers of ice that are the first step in ice formation; grease ice, represented as a slush drink, is a mass of unconsolidated frazil ice; pan ice, represented by a frying pan, are thin pieces of ice that form when grease ice consolidates into solid masses; cake ice, represented by a wedding cake, are typically forms of composite ice, made up of pieces of solid ice and grease ice, frozen together; large ice blocks, represented by a van, are van-sized ice blocks that form when the ice walls in tidal channels collapse during the spring melt. The steps in the formation of ice walls in tidal channels, as represented in the bottom part of this diagram are described in Sections 2.5 and 5.1.

2.1 Introduction to study sites

Ice-formation processes were observed by Paul Hill, Richard Clark, and CarolAnne Black over the winters of 2010/2011 and 2011/2012 (for a map of the locations of study sites, see Figure 1.1). Richard Clark is a retired engineer who helped with this project by providing ice observations and photos from the region around his home, in Summerville, on the Avon River. Hill, Clark, and Black visited several of the tidal channels connected to the Minas Basin throughout the winter. In particular, Hill and Black observed the Kennetcook River site at the bridge near Scotch Village biweekly from October 2011 to May 2012. The sites were also observed outside winter for comparison between winter and ice-free channel morphology. Qualitative observations of seasonal ice formation and changes to channel morphology were noted and documented through photographs. The processes observed corroborate observations described in previous research papers, as will be described in the following sections.

Clark monitored a site in Summerville, along tidal flats near the mouth of the Avon River, and a site at a bridge near Scotch Village, over a narrow section of the Kennetcook River. Four other sites were monitored by Hill and Black. Two sites are along the Shubenacadie River, close to Maitland, along Highway 215: one is at the Fundy Tidal Interpretive Centre in South Maitland, where rock cliffs wall the river and a small tributary connects to it; the other is farther north along Highway 215, in Maitland, at the mouth of the Shubenacadie River, where the banks are gently sloped, and the river is shallow and wide. The other two sites are along the Salmon River: one is near Old Barns, off of Highway 236, where the river is wide and shallow; and the other is at Debert Beach, off of Highway 104, which is an exposed mud and cobble beach at the mouth of the Salmon River and near the mouth of the much smaller Debert River.

2.2 Ice formation - initial stages

The first stages of ice formation in the Minas Basin happen in regions where the water is shallow enough, particularly at low tide, for the whole water column to become super-cooled. This is a requirement of ice formation in waters with strong mixing. Regions where super-cooled water can occur in the Minas Basin are along the tidal flats and at the mouths of the rivers that run into the Basin. The tidal flats region has been termed

Figure 2.2: Examples of grease, pan, and floe ice. (a) In the first stages of ice formation, grease and pan ice cover the surface of the water at the Fundy Tidal Interpretive Centre, along the Shubenacadie River. (b) A close-up of the ice in photo (a), looking down at a thick cover of grease ice and pieces of pan ice. (c) Pan ice covers the surface of the Avon River at Summerville. (d) Floe and pan ice move swiftly upstream with the flood tide. (e) A close up of photo (c), pieces of pan ice show signs of being rounded due to shearing forces, and of having a raised lip around their perimeter. (f) Stranded grease and pan ice at Summerville. As in photo (d), a raised lip is visible at the perimeter of the pieces of ice. Some of the blocks may be thick enough to be classified as cake ice.

an 'ice factory' due to the enormous quantity of ice that forms there. (*Desplanque*, 1967; *Desplanque and Bray*, 1986)

Once the water is super-cooled, tiny fragments of ice, called frazil ice, form in abundance throughout the water column. These ice particles float to the surface and agglomerate,

creating a brown slushy layer of unconsolidated ice, called grease ice (Figure 2.1a and b). (*Desplanque and Bray*, 1986)

Over time grease ice freezes together into pieces of pan ice, which are flat and plate-like (Figure 2.1b and c). Pieces of pan ice are from a few centimeters to about 15 cm thick, roughly round, and about 30 cm to 10 m in diameter. Because the tidal flows in the Minas Basin are energetic, pieces of pan ice experience shearing with surrounding ice that tends to make them nearly circular in shape. (*Gordon and Desplanque*, 1981)

Pan ice and grease ice can freeze together into larger, round and thin pieces of ice called floe ice (Figure 2.1d). Floe ice can have diameters of 50 to 100 m. These large pieces of relatively thin ice form mainly in regions where salinity is low and where turbulence caused by tidal energy is reduced. Floe ice behaves similarly to pan ice. (*Desplanque and Mossman*, 2004)

Pan and floe ice tend to thicken over time. The shearing effect with surrounding ice and wobbling of the ice in the flow tend to cause an accumulation of slush as a raised lip around their perimeter (Figure 2.1e and f). The result is that of creating a shallow bowl or pan. Sediment-laden water can then inundate the pan or floe, making a pool on the top surface. Some of the water will freeze to the ice and become part of it. It has been observed that most of the water, however, will drain through the ice. The sediment that was in the water is left behind. This sieving mechanism increases the sediment content of pan and floe ice. (*Desplanque and Bray*, 1986; *Desplanque and Mossman*, 2004)

The ice - grease, pan, and floe - is transported with flood tides into the upper reaches of the Basin and into its tributaries and then with ebb tides into the open Basin. Ice that flows with the tidal currents is called drift ice. *Sanders and Baddour* (2006) reported that in 2002, by February, Cobequid Bay, in the eastern-most part of the Minas Basin, was more than 90% covered by drift ice. Thirty percent of the drift ice was 10 to 15 cm in thickness and was part of floes that were 20 to 100 m in diameter. Despite this coverage, the whole region never froze over as one solid piece of ice. Tidal currents break up the ice and re-distribute it with each tidal cycle. (*Knight and Dalrymple*, 1976)

2.3 Stranding and the initial stages of ice block formation

As the tide ebbs, ice may become stranded in the intertidal zone (Figure 2.2a). The majority of stranding occurs in the upper reaches of the Basin and in the wider and shallower parts

Figure 2.3: Examples of stranded, composite and cake ice. (a) With ebb tide, ice strands on the banks of the Salmon River. (b) With ebb tide, grease ice, pan ice, and some cake ice strands along the wide, nearly flat banks of the Shubenacadie River. (c) Graduate student Shaun Gelati stands next to a block of composite ice at Maitland. The block is made up of layers of ice pieces, which were stranded one on top of the other throughout a number of tidal cycles. (d) Cake ice blocks are stranded near Old Barns. The water and ice flowing by erodes the bottom and sides of the block until they are rounded, with a smaller diameter near their base, because the base of the block spends more time exposed to flowing water and ice.

of its tributaries. These are the regions where the banks are typically wide and shallowly sloping. (*Desplanque*, 1967; *Gordon and Desplanque*, 1983)

Stranded ice is exposed to freezing air temperatures at low tide. If stranded on muddy sediments, the ice can freeze to the substrate and incorporate a significant amount of sediment into its structure. When the tides rise again, most of the stranded ice will re-float, taking frozen sediment with it. (*Gordon and Desplanque*, 1981; *Hind*, 1875; *Desplanque and Bray*, 1986)

Large volumes of ice can become stranded on the shallow mudflats (Figure 2.2b). Pieces of ice can freeze to other ice, or to the substrate. Pieces of ice may even be rafted on top of

other stranded ice and may freeze to the ice below, making multiple layers of ice. During flood tide, pieces of ice are broken away from the stranded ice formation; however, the new pieces may be agglomerates of previously separate pieces. Ice blocks that formed from the freezing together of multiple other ice pieces are called composite ice (Figure 2.2c). (*Gordon and Desplanque*, 1981)

Over time, more ice forms, and larger pieces of ice form. Pieces of ice that are nearly as thick as they are wide, and can be up to a few meters in size, are called cake ice (Figure 2.2d) (*Gordon and Desplanque*, 1981). As with pan ice, these pieces of ice will tend to take on a rounded shape. Cake ice is large enough that if it becomes stranded, it can remain stranded for a significant portion of the tidal cycle. The bottom part of the ice is exposed to more shearing due to the passing water and ice than is the top part. The result is a cupcake-shaped block of ice, with a smaller diameter bottom and larger diameter top. Large enough pieces of composite ice can become cake ice if they become stranded in an area with a relatively high flow of water and ice, where they can be shaped by the flow around them. Both composite ice and cake ice are instances of ice blocks, which is a general term for larger pieces of ice.

2.4 Ice fields

When stranding occurs, some of the ice will freeze to the substrate and other stranded ice so solidly that it can not be re-floated. In this case, the ice's buoyancy and the eroding power of the tidal currents are not strong enough to overcome the strength of the bond between the pieces of ice and substrate. Formations of ice that are frozen to the substrate are called shorefast ice. The result of a build-up of shorefast ice is an ice field made up of a jumble of blocks (Figure 2.3a). (*Gordon and Desplanque*, 1981, 1983; *Desplanque and Mossman*, 1998)

Incoming tidal currents can be significantly slowed in the region of an ice field, due to friction with shorefast ice (Figure 2.3b and c). The stranded ice also acts as a permeable barrier between the banks and the central flow of a channel, allowing sediment-laden water to pass, but limiting the passage of ice.

The water inundating the ice fields was recently turbulent and capable of suspending significant amounts of sediment. When the flow slows, turbulence in the water column subsides, and ice and sediment can be deposited. The surface of the water freezes as a

Figure 2.4: Examples of ice fields and their their effects on channel flow. (a) Robbie Paterson and CarolAnne Black observe an ice field made of shorefast ice and stranded, layered ice at Maitland. A small tidal channel in front of the students is filled with ice and has a partial ice wall along its banks. (b) Stranded ice along the banks of the Salmon River inhibits the flow of grease and pan ice and fast-flowing water. The open part of the channel is on the left side of the photo and is covered in grease and pan ice. On the right side of the photo, water seeps around blocks and deposits sediment on an ice field. A layer of ice is deposited with ebb tide if the water covering the banks is stationary long enough for ice to form on its surface. (c) As in (b), the inundation of an ice field by slowly moving water (foreground) and ice flowing in the thalweg of the channel (background).

layer, and sediment in the water column settles out and deposits onto the ice below. As the tides recede, the surface layer of ice is deposited onto the layer of sediment (Figure 2.4a). This process can form tidal couplets of alternating sediment and ice layers (Figure 2.4b). Repeated tidal cycles add layers of ice and sediment between the cake ice barrier and the banks, contributing to the growth of ice on the banks. Clear white layers can also be created by snowfall. The presence of high concentrations of sediment on the top surface of shorefast ice was noted by *Gordon and Desplanque* (1981), but the mechanism that caused the deposits of sediment was not described (Figure 2.4c).

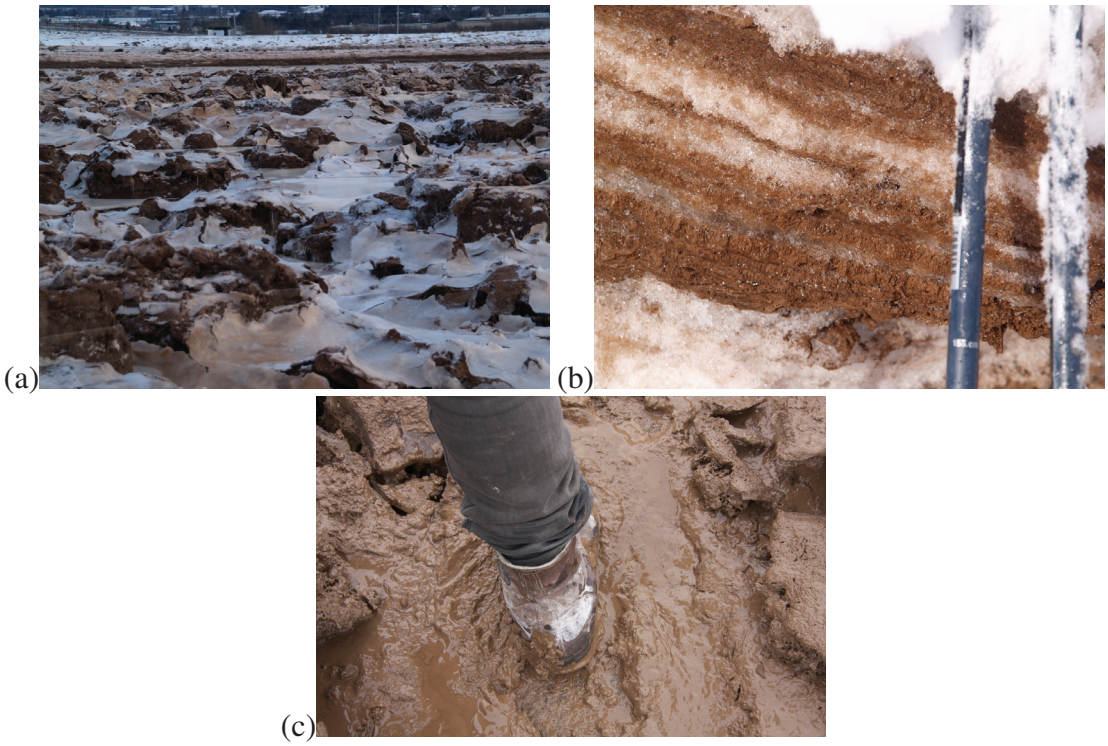

Figure 2.5: Examples of layering of sediment and ice within ice fields. (a) A layer of ice has been deposited on an ice field along the Salmon River. (b) Couplet layers of sediment and ice due to deposition on the ice within an ice field. (c) A thick layer of sediment has been deposited on top of a layer of ice in an ice field. The sediment settled out of the water column at slack tide.

The ice field extends from below the neap high water mark to the spring high water mark (*Gordon and Desplanque*, 1983). Only once the ice field is completely inundated can drift ice, transported with the incoming tide, be floated on top of the ice field and added to it. The level of the tide in the area governs the vertical extent of the ice fields and the buildup of ice on channel banks.

Deposition of ice within an ice field does not mean the ice will necessarily freeze there and remain immobile throughout multiple tidal cycles. Tidal currents can break up the ice that has accumulated on the banks, creating small and large pieces of ice that are moved around the Basin and may be stranded again. Over the winter, however, the result of stranding, re-floating, and becoming shorefast is an accumulation of ice along the banks of the Minas Basin and its tributaries.

2.5 Ice wall formation in narrow tidal channels

In the narrow parts of the tidal channels, the same processes of ice formation and stranding described above result in the formation of vertical ice walls (Figures 2.6 and 2.7a). Ice walls in channels connected to the Cumberland Basin have been reported with heights of up to 5 m (*Gordon and Desplanque*, 1983; *Desplanque and Bray*, 1986; *Desplanque and Mossman*, 1998). The portions of tidal channels where ice walls form have a cross section that is trapezoidal in shape in the summer. The summer bank slopes are about 1:3.5, or a slope of approximately 16°. The winter banks of ice make the channel cross-section rectangular in shape (Figure 2.7a and b) (*Desplanque*, 1967; *Gordon and Desplanque*, 1981).

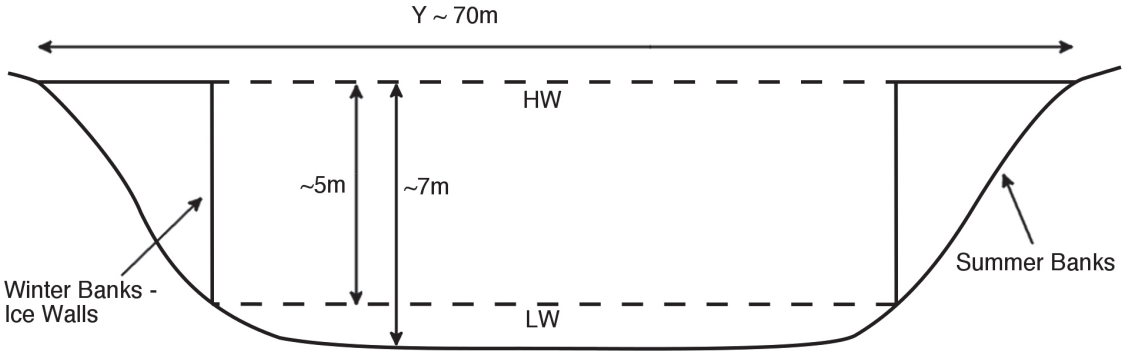

Figure 2.6: Diagram of Kennetcook River channel near the bridge, including the extent of the ice walls and the scale of the channel.

In these regions, the presence of ice walls causes a decrease in the cross-sectional area of the channel that significantly changes the flow of water and ice. A decreased channel cross-sectional area is associated with a reduction in flow speed. (*Desplanque*, 1967; *Gordon and Desplanque*, 1981, 1983; *Desplanque and Mossman*, 1998)

Larger ice blocks are “ratcheted” upstream and add to the formation of the ice walls (*Desplanque and Mossman*, 1998). Ice blocks tend to move predominantly upstream over tidal cycles because the water column carrying the ice can become vertically compressed as it flows into shallow water, so the ice is transported upstream and shoreward until it becomes grounded. Once grounded, the ice becomes less likely to be dragged offshore by the ebb tide. Due to inertia in tidal channels, tidal waters also continue in the upstream

Figure 2.7: Examples of ice wall formation. (a) Winter ice wall conditions along the Kennetcook River. The ice wall is completely developed, with a nearly horizontal upper surface and nearly vertical wall. (b) The same view as in photo (a), during summer conditions. (c) An ice block left a track in the bed as it was "ratcheted", with the incoming tide, up the banks of the Shubenacadie River. (d) A young ice wall along the Kennetcook River accumulated stranded ice blocks, grease ice, and pan ice on its upper surface. (e) Graduate student CarolAnne Black on top of the ice wall at the Kenntcook River bridge. (f) Upper section of the Cogmagun River is frozen over. Note hinges - breaks in the ice - along the banks due to the raising and lowering of the water below with the tides.

direction in tidal channels after the tide in the Minas Basin has changed direction. Ice blocks swept upstream will continue upstream, with the flood tide for a longer period in each tidal cycle, than blocks swept downstream continue downstream with the ebb tide. (*Desplanque and Bray*, 1986)

Ice walls start as porous agglomerations of ice blocks, grease ice, and pan ice: they are irregular in shape (Figure 2.7d). Over many tidal cycles, ice continues to strand in available spaces and water fills in many of the air pockets, then freezes. Grease ice flowing over the top surface of the ice walls tends to fill in gaps in the ice, resulting in a smoothed surface-layer. The deposition of layers of ice and sediment at slack water also help to make the top surface horizontal (Figure 2.7a and e). (*Desplanque and Bray*, 1986) Non-vertical surfaces are locations upon which ice can become stranded, resulting in progressively more vertical ice walls over time. Sometimes they have the appearance of a rock face (Figure 2.7e).

The height of the ice walls depends on the channel tidal range (Figure 2.6). The base of a channel ice wall occurs close to the low water level (*Gordon and Desplanque*, 1983): ice strands and freezes to the bed most easily on substrate that is exposed to the air during part of the tidal cycle. The height of a channel ice wall reaches the high water level. The longer-scale variations of the tidal range affect the extent of the ice walls from year-to-year. The two-week cycle of spring and neap tides, combined with the monthly cycle of the perigean tides (due to the elliptical orbit of the moon), result in a 206-day cycle. When ice wall formation coincides with the second half of the 206-day cycle, the tidal range, and hence the ice walls, will be extremely large. The years where the tidal ranges will be largest in winter are 2016 and 2034 (and most recently, 1998). (*Desplanque and Mossman*, 1998, 2004)

Farther upstream, tidal channels tend to narrow. The ice walls on either bank get closer together (*Desplanque and Bray*, 1986). Where the channel is narrow, the ice walls can touch, or the channel can fill up with ice blocks, and the channel can freeze solid. Over the 2011 winter, the upper section of the Salmon River, beginning near the west end of Truro, froze over completely, and there was no further ice or water action observed until the spring melt.

In the inland reaches of channels, the flow can be dominated by freshwater outflow. In freshwater-dominated parts of the channels the upper layer of water may freeze solid. On

both banks, along the direction of flow of the channel, the ice may crack (Figure 2.7f). This crack is called a hinge. The hinge is created by the effects of the tides, raising and lowering the water level under the ice. (*Desplanque and Mossman*, 1998)

2.6 Formation of large ice blocks

Ice walls in tidal channels can grow to up to 5 m high. The partial thawing of ice walls can cause them to become unstable. There are three main mechanisms that cause thawing: inundation of the banks with above freezing water, rainfall, and melting by the sun, the last of which is exacerbated by the relatively low albedo of the sediment in the blocks. Once significant melting has occurred, the ice walls can fracture and large pieces can break away into the channel (Figure 2.8a and b). (*Gordon and Desplanque*, 1981)

(a)  (b) 

Figure 2.8: Examples of the formation of large blocks from ice walls. (a) and (b) Unstable ice walls collapse, releasing large sediment-laden ice blocks into the channel along the Kennetcook River.

Melting events occur more frequently as spring approaches. In the latter part of February and all of March, the ice walls fracture and lose structural integrity. In particular, the relatively warm tidal waters thaw the bottom of the ice walls, making them unstable by undercutting their base (*Desplanque and Bray*, 1986). At this time *Gordon and Desplanque* (1981) described the channels as having "the appearance of boulder fields". Some of this ice, which at this time of the ice cycle has a very high sediment content (see Section 2.7), will melt in place, but some will also be transported into the Basin. (*Gordon and Desplanque*, 1981)

There are other processes that can form large blocks. *Hind* (1875) states: "At the time

I am now writing, (26th January, 1875), the sandy flats of the Avon are covered with innumerable blocks of mud-ice, daily increasing in dimensions and weight, owing to the prolonged cold weather of the past month." In this statement Hind is referring not to the large blocks that are created by the failure of ice walls, but to other mechanisms. The mechanisms discussed in sections 2.2 to 2.5 can also create large blocks. Ice blocks can accumulate grease ice and pan ice while floating in the water column. The creation of composite ice and the addition of layers of sediment and ice to blocks also aid in the creation of large ice blocks.

2.7 Mechanisms that increase the sediment to ice ratio in ice blocks

Increasing an ice block's sediment-to-ice ratio increases its density. If a block contains enough sediment, it can be neutrally or negatively buoyant. As ice blocks form, sediment from the water column is incorporated into their mass. Once formed, ice blocks are affected by mechanisms that can increase their density, by increasing the ratio of sediment to ice. One mechanism is differential release. As an ice block melts, it preferentially releases water, but retains sediment, which increases its density. Another mechanism is plucking, which sees density increase as additional sediment from the bed freezes to an ice block.

The most observed, by far, of the mechanisms for increasing the density of an ice block is plucking (*Hind*, 1875; *Desplanque*, 1967; *Knight and Dalrymple*, 1976; *Gordon and Desplanque*, 1981; *Desplanque and Bray*, 1986; *Desplanque and Mossman*, 1998; *Sanders et al.*, 2008). Due to the extent of the tidal mudflats in the Minas Basin, plucking can affect the density of a large fraction of ice blocks. *Hind* (1875) describes the quantity of plucking on the mudflats this way: "The spectacle thus presented by an extensive sand-bar after a few hours of freezing weather, is most extraordinary; the whole surface of the flood or ebb becomes suddenly alive with blocks of ice, springing up from below, each carrying away its burden of sand or mud frozen to its base."

Indications of plucking can be observed indirectly. Blocks were observed, while beached, to contain layers of sediment and grass (Figure 2.9a and b). Indentations in sediment substrate, on the banks of the Salmon River, at Debert Beach, were also observed (Figure 2.10a). The indentations were the locations where blocks sat, stranded at low tide. Sediment was incorporated into the blocks and was removed from the banks when the block floated away with rising tidal currents.

(a)  (b) 

Figure 2.9: Examples of plucking, which is a mechanism that increases block density. (a) An ice block at Debert Beach contains grasses and sediment, which are signs of plucking. (b) Inner layers of an ice block at Debert Beach contain a stone. The stone was likely plucked by a block that was then rafted onto another block, creating a composite block with a layer of sediment and grass in its interior.

Composite ice blocks tend to be heterogeneous in density, since they are made up of a number of blocks, each with its own density. Blocks often have the opportunity, through collisions and shearing forces, to fracture. Heterogeneous ice blocks can be subject to fracturing in such a way that the densities of the fractured pieces are different from the density of the initial ice block (Figure 2.10b). The fracturing of heterogeneous ice blocks can increase the density of one or more of the fractured pieces. (*Sanders*, 2011)

Lastly, ice blocks may increase their density through differential release (*Sanders*, 2011). Ice blocks retain sediment and lose water during melting events. Dark brown, high density, blocks have been observed with nearly transparent icicles (Figure 2.10c and d). The loss of water from an ice block increases its density. Differential release may also cause blocks to fracture, which could create a denser part. The effect of melting and refreezing could increase ice block density. Air pockets may be filled with water and sediment that then freezes into ice.

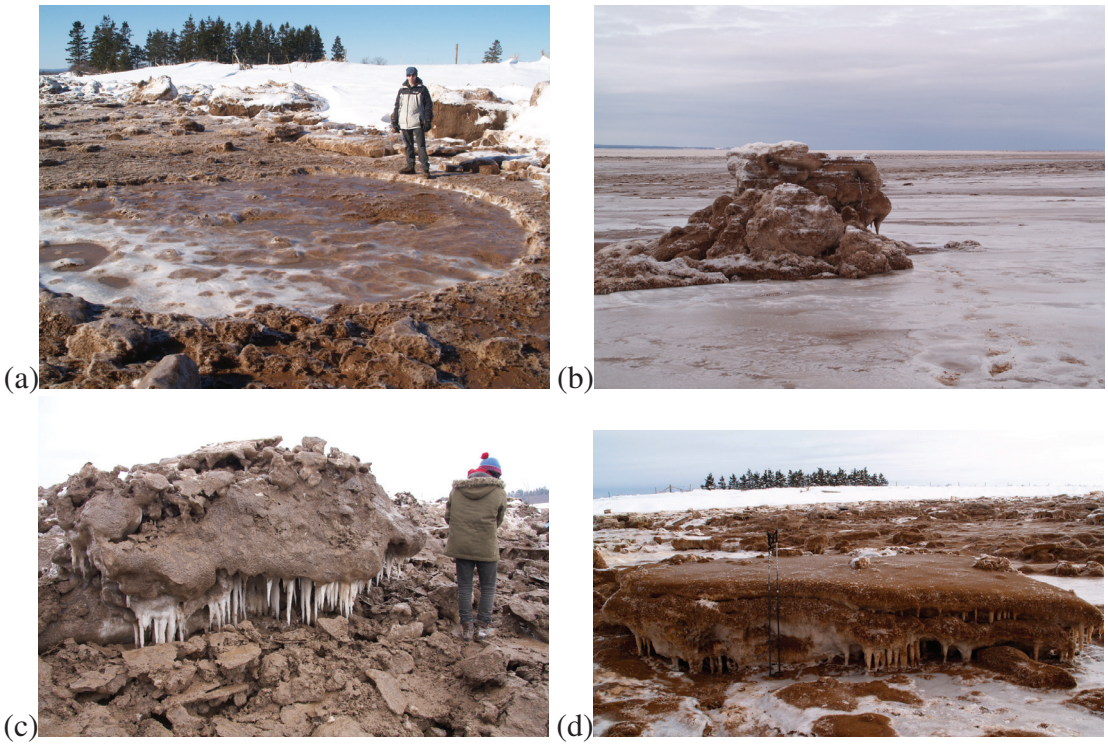

Figure 2.10: Examples of plucking and differential release, which are mechanisms that increase block density. (a) Co-op student Robbie Paterson stands next to an indentation in the sediment at Debert Beach. A large ice block plucked the sediment, incorporating the sediment into its base before being transported away at high tide. (b) A composite block, formed by the fusion of many smaller blocks of differing density, may be fractured while in the water column, to form two or more smaller blocks that may be negatively buoyant. (c) Graduate student Nick Dourado stands next to a block in a relatively wide and shallow part of the Kennetcook River. The block is melting in the air and sun, which creates icicles. The icicles are whiter (less sediment-rich) than the block. The preferential loss of freshwater from the ice block increases the ice block's density. (d) On Debert Beach, another example, as in (c) of differential release that increases ice block density.

2.8 Hypotheses

Two conceptual models were developed as part of this project to represent the change in channel morphology between summer and winter. These end-member hypotheses were tested and the results are reported in Chapter 4 and discussed in Chapter 5. The models are described in this section.

2.8.1 Conceptual Model Introduction

Channels change from their summer morphology to their winter morphology in one of two ways. Channels may retain their summer-time areas and change morphology due to the

change in bank composition, as given by the Modified Bank Materials (MBM) model, or channels may constrict due to reduced flow caused by increased drag imposed by stranded ice, as given by the Modified Friction (MF) model.

Channel morphology is a function of the following variables: channel shape, channel slope, the materials that make up the bed and banks (bed roughness), and the fluid motion in the channel (*Leopold and Maddock*, 1954). Channels, at equilibrium, adjust to perturbations of these variables to form new equilibrium states. The basis of both MBM and MF hypotheses is the assumption that at equilibrium, the peak discharge of the channel and the channel cross-sectional area are linearly related. In that case, the maximum channel velocity in tidal channels is constant.

The study that lead to the adoption of this assumption investigated geomorphic relationships in the Venice Lagoon. Discharge is defined as

$$Q \equiv UA, \tag{2.1}$$

where Q is the discharge (m^3/s), U is the velocity (m/s), and A is the channel cross-sectional area (m^2). *Rinaldo et al.* (1999) measured the cross-sectional area and maximum discharge of tidal channels and found that a linear 1:1 relationship holds for cross-sectional areas between approximately 50 and 5,000 m^2 and for maximum discharges between approximately 50 and 5,000 m^3/s. The *Rinaldo et al.* (1999) result implies a constant maximum velocity within the system of channels. Applying this result to the Kennetcook River system, if the channel's peak flow velocity was perturbed, the channel's morphology would react by changing in a way that allowed it to regain the equilibrium maximum velocity. The new state, however, may not have the same cross-sectional area or discharge as the unperturbed state.

An ensuing underlying assumption is that the flow dynamics affecting the channel are tidally driven and that the freshwater input is small enough to be ignored. The average freshwater input into the Bay of Fundy and Gulf of Maine accounts for approximately 0.045% of the tidal prism of an average tide (*Desplanque and Mossman*, 2004). This thesis does not include measurements of tidal and fresh water inputs into the Kennetcook River. However, based on the fractions of freshwater input into the Bay of Fundy, the freshwater input into the Kennetcook River is likely relatively small, so the assumption is taken to be valid.

2.8.2 Model 1: Modified Bank Materials

Channel bank steepness is governed by bank materials (grain size and cohesivity), as well as the shear stress exerted by water on the banks (*Leopold et al.*, 1995). Steeper banks are associated with higher cohesivity. For instance, *Schumm* (1960) showed a direct relationship between the percentage of the bank material made up of silt/clay and the depth-to-width ratio of the channel. Furthermore, *Istanbulluoglu et al.* (2005) found that gullies that possess more cohesive bank materials form deeper, more vertical walls than do gullies formed by less cohesive bank materials. *Anderson et al.* (2004), *Gran and Paola* (2001), and *Hickin* (1984) also found that vegetation increases the cohesivity of the soil and that channels with vegetated banks are deep and narrow. These studies show that channels made from more cohesive material are narrower and have steeper banks. According to the MBM hypothesis, the change in bank material from less cohesive mud in summer to more cohesive ice-mud mixtures in winter is what drives the change in channel morphology: channels go from wide and shallow to narrow and deep, and bank angles go from gentle to steep.

Discharge in a tidally-driven channel is determined by the tidal pressure gradient force (*Garrett and Cummins*, 2005). When ice forms on channel banks the channel area overlying those banks is reduced. The velocity must increase enough to cause erosion that deepens the channel to compensate for the reduced width. The decrease in channel width over banks was observed by *Gordon and Desplanque* (1983), however their observations did not include depth measurements. In the MBM hypothesis, the channel should deepen to return the cross-sectional area to its original value, despite the apparent constriction in the width.

Since channel flow velocity is proportional to grain size eroded (*Wiberg and Smith*, 1987), the grain size distribution of the top layers of the bed should change in response to changes in velocity. When the velocity increases, the channel deepens and the grain size increases. But, as the channel deepens, the cross-sectional area increases, and the velocity decreases. The velocity will continue to decrease until the equilibrium velocity has been reached. Changes in grain size occur as follows: at the onset of winter, grain sizes should increase; as the channel reaches its winter equilibrium grain sizes should decrease to the equilibrium value; as the ice melts grain sizes should briefly decrease further before increasing to their equilibrium size (Figure 2.11).

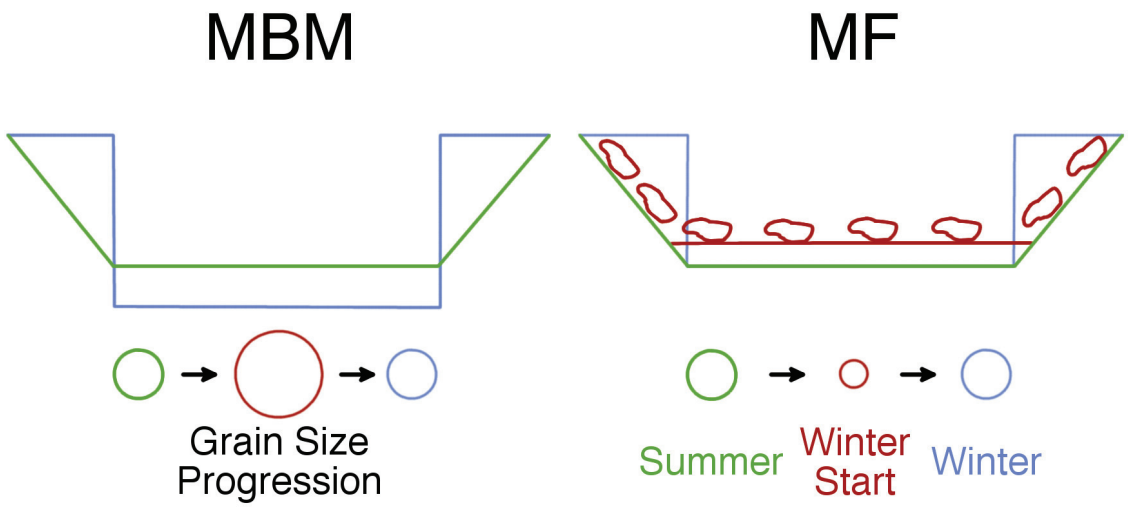

Figure 2.11: Changes in channel morphology in winter, due to Modified Bank Material and Modified Friction hypotheses. Green, red, and blue represent the states of the channel during summer, at the onset of winter conditions, and winter, respectively. Circles represent relative changes in grain size during the three periods.

2.8.3 Model 2: Modified Friction

According to the MF hypothesis, increased friction in tidal channels due to the presence of ice spurs a change in channel morphology. The force balance equation for tidally-driven channel flow is as follows (*Campbell et al.*, 1998):

$$-g\frac{\partial \eta(t)}{\partial x} = \frac{k|u(t)|u(t)}{h'(t)} + \frac{\partial u(t)}{\partial t}, \tag{2.2}$$

where g is acceleration due to gravity, $\partial\eta(t)/\partial x$ is the along-channel surface slope, x is the along-channel coordinate, $u(t)$ is the depth-averaged velocity in mid-channel, k is the bottom drag (frictional) coefficient, and h' is the water depth equal to $d(y) + \eta(t)$, where $d(y)$ is the channel depth and $\eta(t)$ is the surface height. On the lefthand side of the equation is the pressure gradient force: the surface slope, multiplied by the restoring force, gravity, determines the strength of the force in the downslope direction. The first term on the righthand side is the bottom stress, which is the dominant term balancing surface slope, given as a quadratic drag law. *Campbell et al.* (1998) found the second term on the righthand side ($\partial u(t)/\partial t$) to be small (less than 5 % of the surface slope term) most of the time. The only exception occurred during rapid changes from flood to ebb tide. The addition of ice to the bed and banks of tidal channels increases friction and by this

equation, increasing friction causes the drag coefficient (k) to go up; to compensate, either velocity must go down or the sea surface slope must steepen.

By equation 2.1, keeping the cross-sectional area constant, decreasing velocity causes a proportional decrease in discharge. As velocity decreases, deposition occurs and more water freezes to the already-present shorefast ice. As channel area constricts with increasing deposition and outward growth of ice banks, velocity is eventually restored to its equilibrium value. The new cross-sectional area remains approximately constant throughout the winter. In early spring, velocities in the channel decrease as the ice melts and the channel widens. The number and size of anchored ice blocks decrease, which together cause the channel velocity to increase due to decreased drag. Once the channel is ice-free, friction with the banks is less, and the channel returns to its summer equilibrium and morphology. Changes in grain size occur as follows: at the onset of winter grain sizes decrease; as the channel reaches its winter equilibrium grain sizes increase; as the ice melts grain sizes briefly decrease further before increasing to their equilibrium size (Figure 2.11).

2.9 Summary and Objectives

Sediment-laden ice forms in the upper Minas Basin. The largest ice blocks typically form in narrow tidal channels, as observed by Black, Hill, Clark, and *Gordon and Desplanque* (1981). Ice blocks may increase their density through differential release and plucking, and may become neutrally or negatively buoyant. Two end-member hypotheses were developed to describe the change in channel morphology that occurs in the winter and leads to the formation of ice walls, and later, to the formation of large sediment-laden ice blocks.

The objective of this thesis is to increase the understanding of large sediment-laden ice block formation mechanisms. To achieve this objective, ice bank processes and properties in the Minas Basin tidal channels are investigated, and the hypotheses described in the previous section are tested. The methods of investigation are discussed in the following chapter.

CHAPTER 3

METHODS

This project involved two types of observational effort. The first was monitoring channel geometry to quantify the volume of ice formed in a tidal channel. The second was sampling ice to quantify the composition and density of ice blocks and ice walls. The primary study site over the 2011/2012 field season was a narrow part of the Kennetcook River, at a bridge near Scotch Village (here called Kennetcook River bridge). This chapter describes the methods for data collection and analyses, as well as the methods for uncertainty determination. Unless otherwise noted, uncertainty calculations were conducted following *Taylor* (1997).

3.1 Channel morphology

The variable of interest regarding channel morphology is the cross-sectional area. To measure the channel cross-sectional area, the Kennetcook River was profiled over time at the bridge site. It is anticipated that the channel cross-sectional area may change from fall to winter and from winter to spring. Depth in the main section of the channel may also change at the onset and at the end of winter.

A weighted measuring tape was lowered from equidistant positions across the width of the bridge. The profile was measured on 18 separate days, approximately weekly over the winter and biweekly outside winter, between October 2011 and May 2012 (Table 3.1). All measurements of depth were taken at low tide, from the base of the bridge railing, and at positions along the bridge that were identified by vertical bars along the railing.

The vertical extent of the channel was determined using measurements of the high high water level. The high high water level was identified as the limit where grasses have

Table 3.1: Dates of visits to the Kennetcook River site over the 2011 to 2012 field season

Month	Day(s)
October	19
November	3, 10, 13
December	20
January	9, 16, 19, 25
February	2, 10, 16, 27
March	5, 14, 25
April	12
May	8

sediment deposits on them from the previous spring tide. The approximate high high water level was measured during a time of spring tides (on February 8, 2013) on both sides of the channel: 4.59 m on the north side and of 5.55 m on the south side. The bridge was assumed to be planar and the difference in high water measurements was used to calculate the slope of the bridge. The bridge slope was accounted for in profile measurements by assuming a linear increase in vertical height above the mean water level progressing from the north side of the bridge to the south side of the bridge. To calculate the actual channel depth ($d(y)$), the height from the high water mark to the bridge was subtracted from the total measured depth ($d_m(y)$):

$$d(y) = d_m(y) - y \tan \phi - h, \tag{3.1}$$

where y is 78.4 m, the distance between the two high water marks, $\tan \phi$ is the tangent of the bridge slope and ϕ is 0.8° (Figure 3.1), and h is the height to the high water mark on the north side of the bridge. From channel depths calculated as above, channel cross-sectional area was calculated using the trapezoid rule.

Changes in cross-sectional area over time were used to develop criteria for determining the timing of the formation and deterioration of the ice walls. January 9, 2012, was chosen as the date of the start of ice walls formation since it was on that field date that ice walls were first observed in the channel. Ice walls have been observed to deteriorate in a relatively short amount of time. The date before a rapid increase in channel cross-sectional area was used as the date for ice walls collapse, which was February 16, 2012.

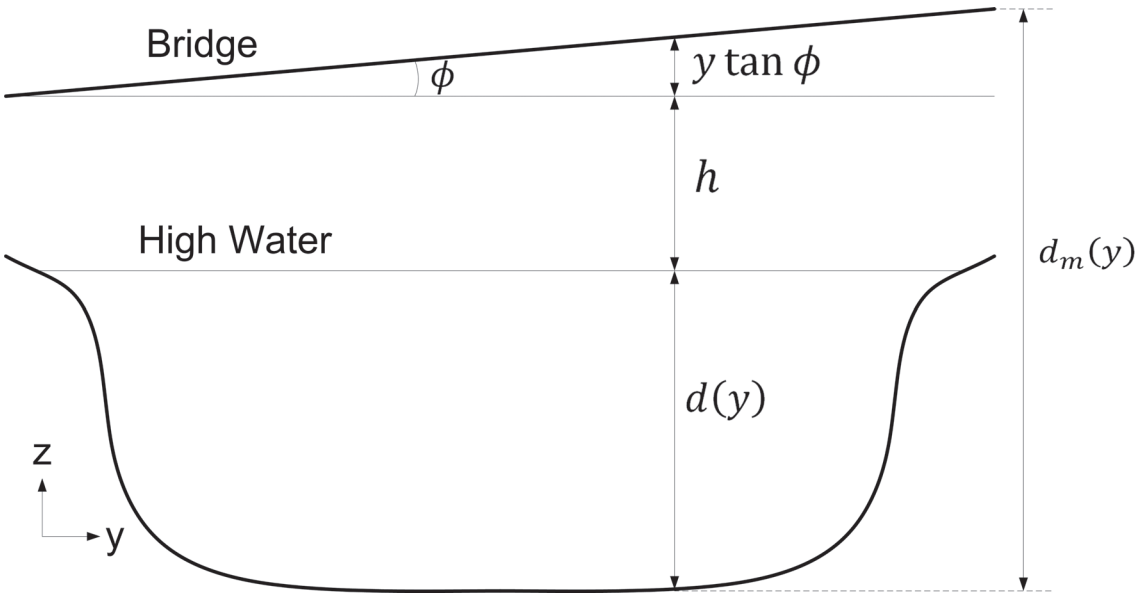

Figure 3.1: Diagram of Kennetcook River bridge and channel, including distances along the bridge and to the channel. Distances used for depth measurements and calculations.

3.1.1 Uncertainties

Uncertainty in the channel depth measurements was determined from channel profiles taken on December 20, 2011, when the winds were strong. At the time of measurement, in the early afternoon, the windspeed for December 20 was 26 km/h, as compared to the average windspeed over the field season of 11km/h. To check the repeatability of the depth measurements in adverse conditions (high winds cause the measuring tape to bow out, which adds uncertainty to the measurements), the profile was taken twice: proceeding from north to south and then from south to north. The average difference between the pairs of depth measurements, between those taken while going south and going north across the bridge on a windy day, is a conservative upper estimate of uncertainty. The uncertainty in depth measurements was $\pm$0.11 m.

The vertical uncertainty of $\pm$0.11m is used for profile plots and cross-sectional area calculations. Uncertainty in cross-sectional area (A_u) is given by the uncertainty in the trapezoid method:

$$A_u = \frac{Y}{\sqrt{N}} d_u(y) \tag{3.2}$$

where Y is the total width of the channel (95.05m), V_u is the uncertainty in the channel depth, and N is the number of measurements across the width of the bridge (41) (*Cox and*

Harris, 2006). At the Kennetcook River bridge, A_u= $\pm$1.78 m^2.

3.2 Sediment

The presence of ice in tidal channels affects flow speed, which is linked to the formation of abundant sediment-laden ice on channel banks and flats (Chapter 2). Measuring flow speed while the ice is present is not practical because moving ice can easily destroy instruments deployed in the channel. A proxy for flow speed is sediment grain size (*Wiberg and Smith*, 1987). To assess changes in flow speed, sediment was collected from the Kennetcook River bridge.

An Ekman grab was lowered from the bridge onto the channel bed at nine positions, at 4.7 m intervals, to collect sediment samples. The Ekman grab closes around the top layers of sediment, which are enclosed as they are brought back up to the top of the bridge. Sediment samples were transferred into labeled sealable plastic bags. During the 2011 to 2012 field season, 66 samples were collected.

Grain size analysis was conducted following *Carver* (1971). The samples were oven-dried at no more than 50 °C. The entirety of each sample was used in the sieve analysis and sample sizes ranged between 0.014 kg and 1.301 kg, with an average of 0.315 kg. The differences in sample sizes are due to the changing conditions at each position across the bridge and over time. For instance, some attempts to collect sediment brought back mostly frazil ice that had frozen to the bed. Each sample was sieved for ten minutes using a Ro-Tap sieving machine. A stack of seven sieves was used.

The median grain size was calculated at the nine positions, and the median of those results - the median grain size across the width of the channel - was plotted over time. To estimate median grain size at each position, a linear interpolation was used between the known sample fractions that passed through each sieve. In five of the samples, median grain size could not be calculated from within the set of sieves because the sediment was too coarse for the range of sieve sizes used.

3.2.1 Uncertainties

During the drying process, even at a low oven temperature, a layer of sediment - likely clay - often formed on the top of the sediment samples (Figure 3.2). It was difficult to break it up completely. As a result, some of the fine material remained in aggregates that were

caught by the largest sieve. However, the sediment caught in the largest sieve typically accounted for less than 5% of the sample's total mass and the majority of it, based on visual inspection, consisted of sand or bits of woody debris. The error introduced by retention of fines was likely in the range of fractions of a percent.

Figure 3.2: A thin layer of small grain size sediments formed on top of a sediment sample as it dried at 50 °C.

Uncertainty in the mass fractions measured after sieving was calculated by comparing the results of three replicates. Three sub-samples of 400 g each were separated from one sediment sample and sieved. The standard deviation of the three replicates, for each size class were calculated (Table 3.2). For each of the replicates d_{50} was calculated, with an average of 98 μm. The replicates of d_{50} differed by less than 1 μm, but the spatial variability across the width of the channel is large.

3.3 Ice

The variable of interest for the properties of the ice is whether it is positively or negatively buoyant. For ice block samples, there is also an interest in knowing if buoyancy can change from positive to negative during melting events. The density, buoyancy, and changes in both can be determined from samples collected from ice blocks and ice walls.

Table 3.2: Three sieve replicates

Sieve size (μm)	Mass replicate 1 (g)	Mass replicate 2 (g)	Mass replicate 3 (g)	Mean mass (g)	Standard deviation (g)
180	7.31	6.19	7.54	7.01	0.590
150	6.52	6.24	6.04	6.27	0.197
125	66.00	65.17	55.50	62.22	4.776
106	72.09	73.06	83.53	76.23	5.179
90	95.29	101.04	97.93	98.09	2.350
75	41.94	38.08	37.10	39.04	2.089
63	37.18	38.11	37.50	37.60	1.164
0	73.13	71.65	74.50	73.09	0.074

3.3.1 Ice block samples

Twenty-six ice block samples were collected over winter of 2011 at sites along the Salmon and Shubenacadie Rivers (Table 3.3). Fourteen were collected over winter of 2012 at sites along the Kennetcook and the Shubenacadie Rivers (Table 3.4). Samples were collected by knocking pieces off the side of ice blocks with a hammer. Dark-brown ice blocks were sampled because sediment-laden blocks are the focus of this study.

Table 3.3: Ice block samples collected in 2011

Date	Samples	Site
February 10	3	Debert Beach
March 3	9	Old Barns
February 17	9	Debert Beach
March 17	4	Debert Beach
March 17	1	Tidal Bore Road

Table 3.4: Ice block samples collected in 2012

Date	Samples	Site
February 2	1	Kennetcook River bridge
February 16	3	Kennetcook River dyke
February 16	4	Kennetcook River bridge
February 27	2	Maitland
March 5	4	Kennetcook River dyke

The volumes of 13 samples from 2011 were determined using a water displacement apparatus (Figure 3.3). The volumes of 4 samples from 2012 were also determined using

the same method, but with a different displacement apparatus. Before immersion in water, the samples were weighed. Densities were determined by dividing block mass by displaced volume.

Figure 3.3: The water displacement apparatus with a sample block that has sunk in the fresh water. The block is contained within a mesh bag.

The water displacement apparatus was a water tank with a valve near the top. The tank was filled with tap water to above the level of the valve. The valve was opened and any water above the level of the valve was drained. The ice block was weighed and put in a mesh bag (which allowed for easy retrieval of the blocks that had a negative buoyancy). The valve was closed and an ice block was put gently into the water. After the introduction of the ice block, the valve was opened and the water displaced by the ice block and the mesh bag was drained into a receptacle. The displaced water was weighed and multiplied by the density of water (1000 kg/m^3) to get the ice block volume. Using these measurements, the densities of the blocks were calculated. Care was taken to minimize the melting of the ice during the procedure. Samples were out of the freezer and immersed in the water for as little time as possible.

A melting experiment was conducted using the remaining 13 samples from winter 2011

and the remaining 10 samples from winter 2012. The experiment artificially reproduced the freeze-thaw cycles an ice block may experience. Samples, which were generally 2 kg or less, were submerged in a tank of freshwater. Qualitative observations of buoyancy were recorded. The samples were then left to melt in a refrigerator at 4 °C for a period of, typically, 6 hours and then refrozen. The cycle of observing buoyancy, followed by a period of melting and then a period of freezing, was repeated until the samples had melted completely. The qualitative buoyancies of the samples were analyzed to determine changes during the melting process.

3.3.2 Ice cores

Ice samples were taken directly from the ice wall adjacent to the Kennetcook River bridge (Table 3.5). Samples were collected using a Kovacs Mark III corer. Cores were up to 1 m in length and 7.5 cm in diameter. Using the corer, samples were collected by hand drilling straight down into the ice for depths up to about 2 m. The depth of sampling was usually greater than the length of the corer barrel because there were many air pockets in the ice. Ice cores were collected on February 2, 10, and 16, of 2012.

Table 3.5: Ice core samples collected in 2012

Date	Samples	Site
February 2	4	Kennetcook River bridge
February 10	5	Kennetcook River bridge
February 16	3	Kennetcook River bridge

The ice cores were drilled from ice walls that lacked structural integrity, so it was not possible to estimate volume accurately. As a result, maximum possible ice block densities were calculated from the mass fractions of ice and of sediment in the ice cores, by assuming a negligible air volume, and by estimating the densities of the ice and sediment. The cores were weighed, melted, and dried. The mass of the sediment was then determined. The maximum density of the ice cores was calculated assuming, for a lower bound, that the ice was made from fresh water (916.7 kg/m^3) (*Haynes*, 2012) and for an upper bound, from seawater. The density of first year sea ice (from below the waterline) has been reported as ranging from 900 kg/m^3 to 930 kg/m^3 (*Timco and Frederking*, 1996). The top of the range was used to give an upper bound to the ice density. Sediment was assumed to be quartz, which has a density of 2650 kg/m^3 (*Haynes*, 2012).

Using volume, mass and density relationships, an equation for the maximum possible density of the cores was developed:

$$\rho = \frac{M_t \rho_i \rho_s}{\rho_s (M_t - M_s) + \rho_i M_s} \ , \tag{3.3}$$

where M_s and M_t are the known mass of sediment and total mass of the ice block, ρ_i, ρ_s, and ρ are the assumed densities of ice, sediment, and ρ is the maximum possible core density, respectively.

Using a similar equation to 3.3, the minimum sediment fraction by mass required for air-free ice to be neutrally buoyant in Minas Basin waters was calculated:

$$\frac{M_s}{M_t} = \frac{\rho_s}{\rho_w} \left(\frac{\rho_w - \rho_i}{\rho_s - \rho_i} \right) * 100\%, \tag{3.4}$$

where ρ_w is the assumed density of seawater. Water density in the Minas Basin is assumed to be 1025 kg/m^3 (*Cornett et al.*, 2011). For freshwater air-free ice, the sediment mass fraction required for neutral buoyancy is 16%. For seawater air-free ice, it is 14%.

3.3.3 Uncertainties

3.3.3.1 Ice block samples

The 13 largest samples from winter 2011, with an average mass of 8.7 kg, and the 4 largest samples from winter 2012, with an average mass of 5.0 kg, were used for density calculations. The densities of smaller ice block samples have large uncertainties due to their size relative to the water displacement apparatus. Small ice blocks cause a small change in the apparatus water level, which makes the volume uncertainty of the collected water relatively large. The density measurements of blocks of approximately 2 kg in mass or less were unreasonable and discarded. For example, a relatively small ice block sample may have floated, yet the calculated density was greater than that of water. The densities of the larger blocks were reasonable in that they were negatively buoyant when their densities were greater than that of freshwater and they were positively buoyant when their densities were less than that of freshwater.

The original apparatus was accidentally discarded during a laboratory cleanup before characterization of error could take place, and the second apparatus was altered before characterization of error was conducted. Uncertainty estimates should be made by doing

replicates of density calculations using a standard object with a known mass and volume. However, even using such an object and calculating uncertainties would only give minimum uncertainty estimates. Uncertainty in ice block density is difficult to constrain because the ice blocks change in mass and volume when they are out of the freezer and immersed in water. Ice blocks melt, lose sediment, and air pockets may fill with water during immersion.

3.3.3.2 Ice cores

The maximal ice density calculations are estimates. Error can derive from incorrectly assumed densities for ice and sediment, or it can derive from weighing the sediment and the sediment-laden ice.

3.4 Environmental measurements

Temperature (T), tidal range, wind, and precipitation are environmental variables that affect the formation of sediment-laden ice. Hourly temperature and windspeed data was downloaded for Kentville, Nova Scotia (Figure 1.1), from the Environment Canada website for October 2011 to May 2012 (*Environment Canada*, 2013). Daily precipitation (the sum of water precipitation and the water equivalent of snowfall) was downloaded for the same period. The Kentville, Nova Scotia, is the nearest Environment Canada weather station to the Kennetcook River bridge, at approximately 40 km from the field site. Tidal data predictions were provided by the Canadian Hydrographic Service for Hantsport, Nova Scotia. (Figure 3.4)

Since ice forms when air temperatures are below zero, air temperature is a useful proxy for the quantity of ice formation. The timing of the onset of predominantly below-freezing temperatures and predominantly above-zero temperatures can be used in predicting the beginning and the ending of ice conditions, respectively. To determine the timing of ice formation and ice retreat, a spline was applied to air temperatures over the study period.

3.4.1 Uncertainties

Environment Canada reports the uncertainties in hourly temperature, daily precipitation, and hourly winds at the Kentville weather station as 0.1°C, 0.1 mm, and 0.1 km/h, respectively. There is also uncertainty due to the distance between the weather station, or the site of tidal predictions and the field site, where conditions may be slightly different.

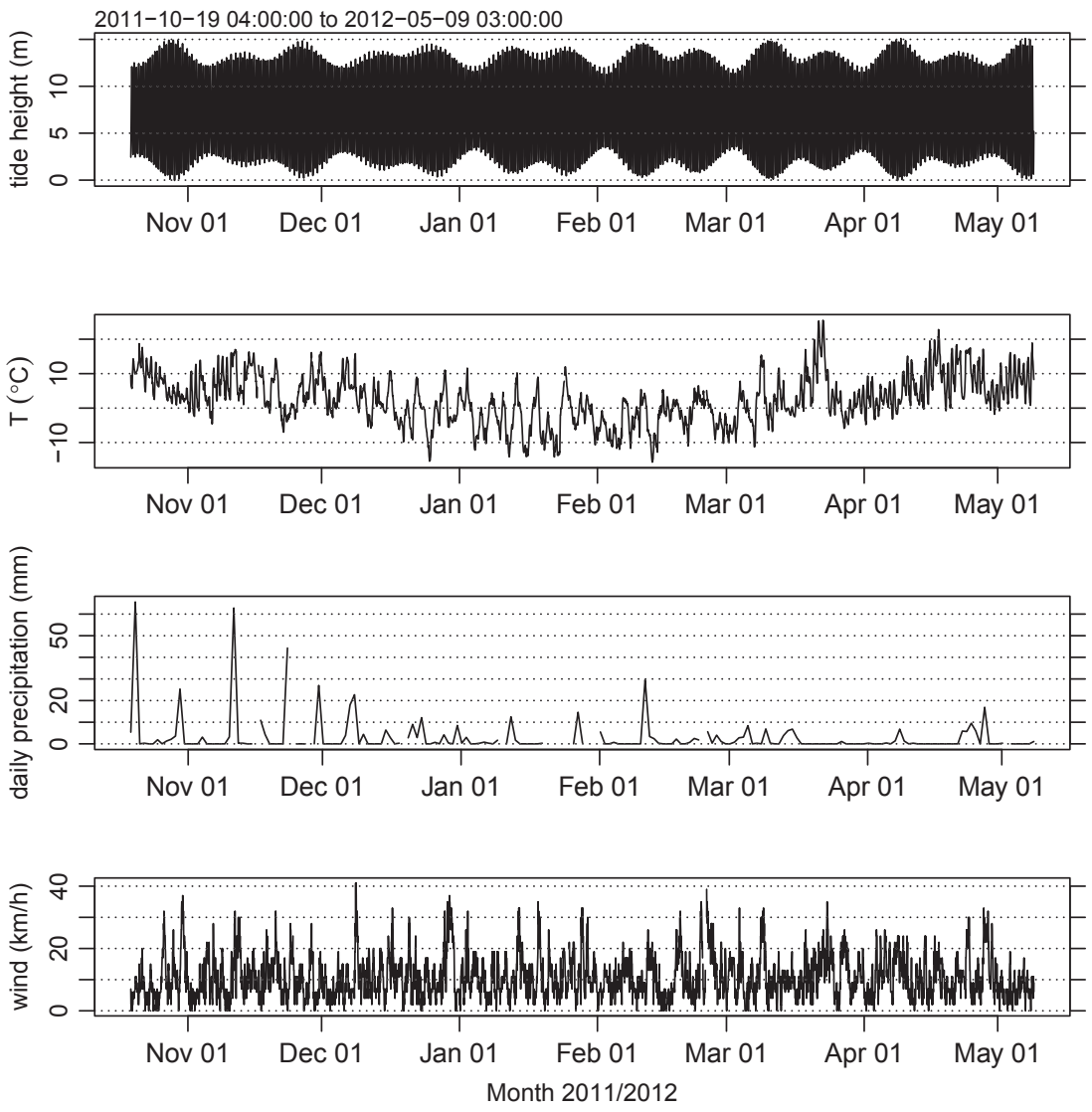

Figure 3.4: Environmental data over the study period: October 19, 2011 to May 8, 2012. Top panel: tidal predictions at Hantsport, Nova Scotia. The bottom three panels: temperature, daily precipitation, and windspeed data from Environment Canada's Kentville weather station.

The tidal predictions themselves have inherent uncertainty in that they are predictions and not measurements. Fisheries and Oceans Canada estimates the uncertainty in the tidal predictions of up to 70 cm. Since Fisheries and Oceans Canada does not report tidal levels for Hantsport, the uncertainty in the tidal predictions can not be further constrained here.

Statistical correlation between temperature and channel cross-sectional area was not calculated. A more accurate result could be achieved to demonstrate the covariance of

the two data sets if the number of cross-sectional area data points over the period were increased dramatically, which was not possible due to time constraints. Fortunately, the sparse data are adequate to assess visually that there is a correlation.

CHAPTER 4

RESULTS

Results relating to the changes in channel morphology during winter, which test the end-member hypotheses developed in this project, are presented in this chapter. Then, the results relating to the composition of ice blocks over two seasons and of ice cores from one season are presented. Lastly, a relationship between temperature and channel cross-sectional area is presented.

4.1 Channel morphology

The shape of the channel profile changed from summer to winter. The channel constricted by narrowing the banks (Figure 4.1). At the onset of winter the depth in the main thalweg remained approximately the same as in the fall, and (Figure 4.2). A reduction in channel cross-sectional area occurred in mid-winter (Figure 4.2). Between the summer average of 408.47 $\pm$1.78 m^2 and the winter minimum of 323.98 $\pm$1.78 m^2 there was a 21% reduction in the channel cross-sectional area. Over the 2011 to 2012 season the cross-sectional area taken up by ice did not attain a maximum for a prolonged period. The cross-sectional area decreased throughout winter until mid-February, then it increased until it reached its summer state. The channel cross-sectional area during winter and outside winter both fall within the range of the linear relationship found by *Rinaldo et al.* (1999) (Section 2.8).

To understand the natural variability of the channel outside of winter, four profiles were taken in the fall: two near neap tide, one near spring tide, and one the day after a major rain event (Figure 4.3). In ice-free conditions the channel profile remains relatively constant.

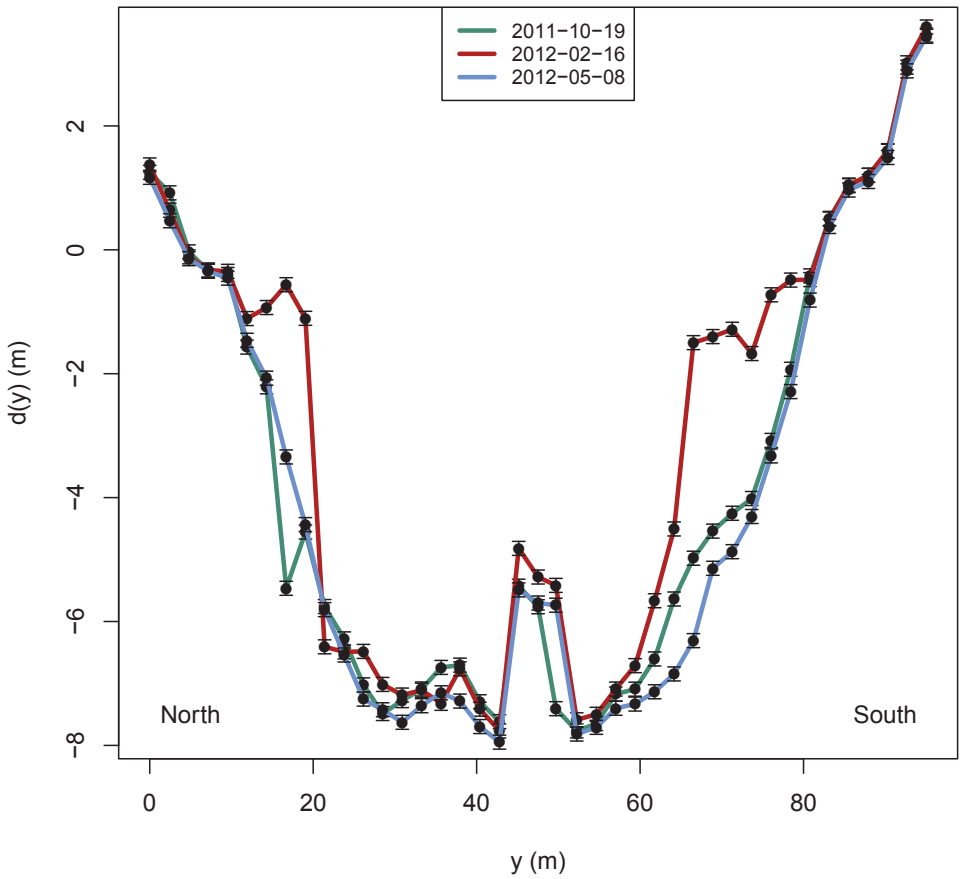

Figure 4.1: Kennetcook River channel depth (y) versus across-channel coordinate ($d(y)$) in fall, winter, and spring of 2011 to 2012. The lesser depth in the centre of the channel is due to the presence of a bridge footing. The red line (2012-02-16) shows the ice walls protruding into the channel. The leftmost approximately ten and the rightmost approximately twenty meters are outside the waterway of the channel.

4.2 Sediment

The trend that emerges from the overall set of sediment samples indicates the fining of the bed sediments during the winter (Figure 4.2). There is a decrease in the median grain size at the onset of winter, beginning in late January and continuing through to mid-March, which indicates deposition in the channel. The median grain size then increases toward the end of March and into April.

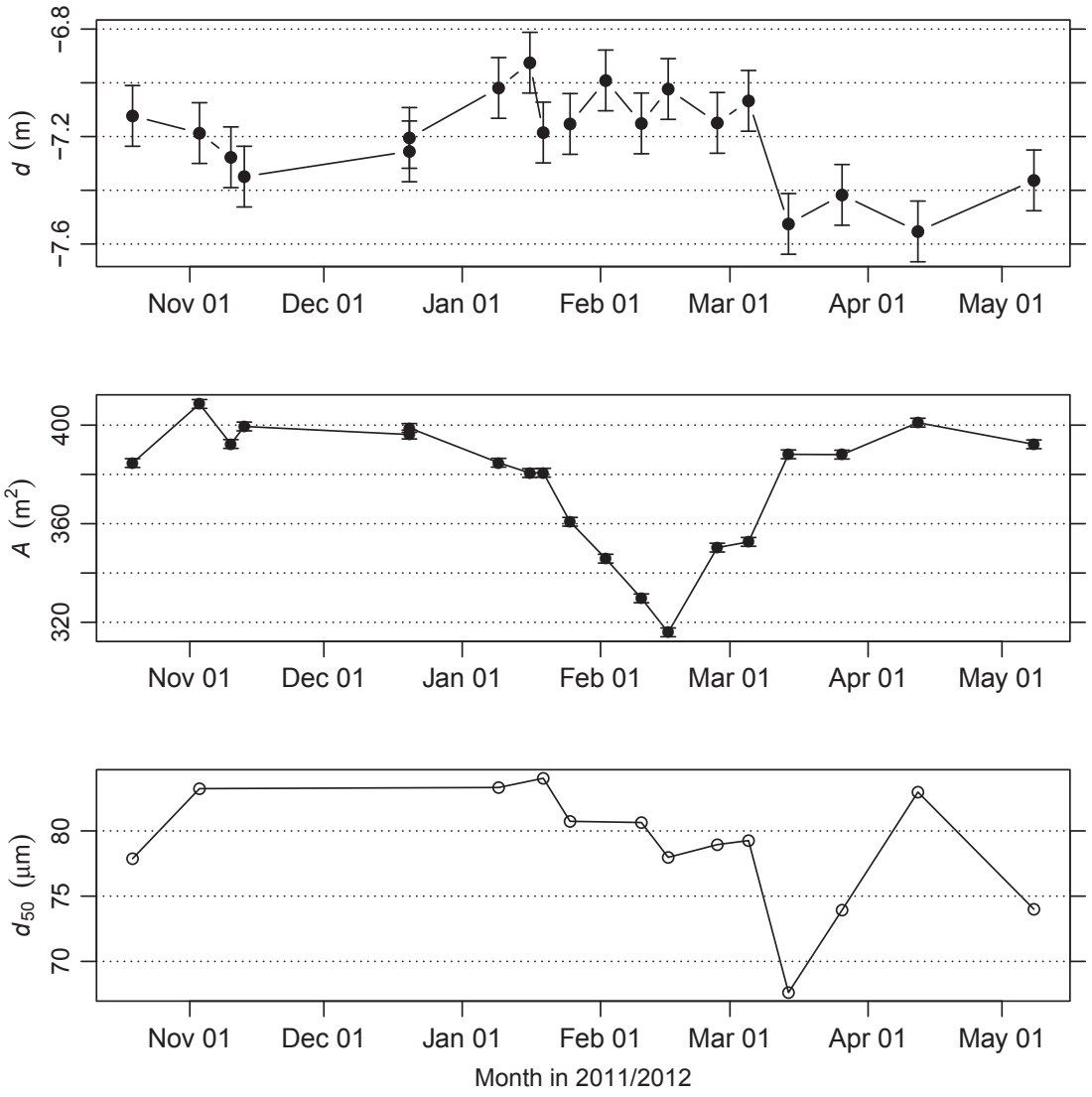

Figure 4.2: Kennetcook River thalweg depth, cross-sectional area, and grain size, from October 2011 to May 2012 at the bridge site. Top panel: mean depth in the Kennetcook River main thalweg (positions from 26.15 to 35.66 m across the bridge). Middle panel: Channel cross-sectional area, calculated using the trapezoid method. Bottom panel: median sediment grain size (d_{50}) over nine positions across the Kennetcook River bridge. Uncertainty in d_{50} measurements is less than 1 μm, but the spatial variability across the width of the channel is large.

4.3 Ice

4.3.1 Ice block samples

The densities of 13 samples collected in winter 2011 were measured (Table 4.1). Samples 9 and 10 had densities greater than freshwater. The volume of sample 12 was measured

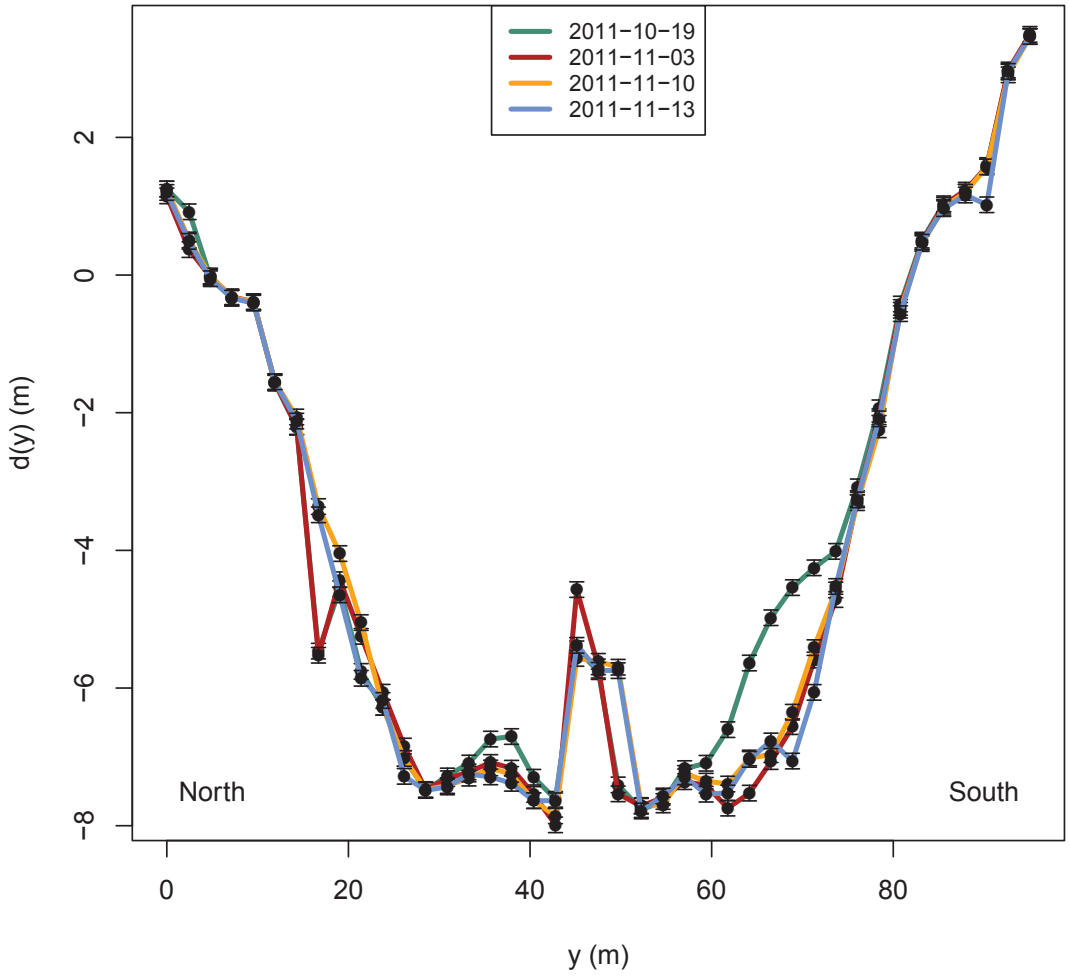

Figure 4.3: Kennetcook River channel depth (y) versus across-channel coordinate ($d(y)$) on four dates in fall of 2011, showing variability of profile outside winter.

twice: initially (sample 12A), and after it had been left to melt for approximately 18 hours (sample 12B). The density of the sample before the melting event was less than that of freshwater, but was greater than freshwater afterward. The densities of 4 samples collected in winter 2012 were measured (Table 4.2). Sample 10 had a density greater than freshwater.

A melting experiment was performed with a set of 23 blocks (13 from 2011 and 10 from 2012), all of which floated at the start of the experiment. The blocks were completely

Table 4.1: Ice block densities from 13 samples collected in Winter 2011. Uncertainty in Sediment mass percentage is a fraction of 1%.

Block number	Date collected	Site	Density (kg/m^3)	Sediment mass percentage	Air volume percentage
1	February 10	Debert Beach	834	8	14
2	February 10	Debert Beach	991	14	2
3	February 17	Debert Beach	914	12	8
4	February 17	Debert Beach	854	1	8
5	February 17	Debert Beach	866	12	13
6	March 3	Old Barns	766	unknown	unknown
7	March 3	Old Barns	831	2	11
8	March 3	Old Barns	822	4	13
9	March 17	Debert Beach	**1108**	31	4
10	March 17	Debert Beach	**1179**	37	3
11	March 17	Debert Beach	963	20	9
12A	March 17	Debert Beach	941	14	7
12B	March 17	Debert Beach	**1017**	18	2
13	March 17	Maitland	955	18	8

Table 4.2: Ice block densities from 4 samples collected in Winter 2012

Block number	Date collected	Site	Density (kg/m^3)
5	February 16	Kennetcook River bridge	759
9	February 27	Maitland	**1033**
10	February 27	Maitland	751
11	March 5	Kennetcook River dyke	778

melted in 3 to 9 melt cycles. None of the samples were found to change buoyancy from positive to negative throughout the experiment.

4.3.2 Ice cores

Twelve ice cores were collected from the Kennetcook River ice walls over three dates in February 2012 (Table 4.3). By assuming ice densities of both freshwater (917 kg/m^3) and seawater ice (930 kg/m^3), and a sediment density of quartz (2650 kg/m^3) and an air volume of zero, a range of maximum ice block densities were calculated. Samples 1, 2, 3, and 4, if made using fresh water ice, could achieve densities greater than freshwater, and samples 1, 3, and 4 of them could achieve densities greater than seawater (assuming a

sea water density of 1025 kg/m^3). Samples 1 through 5, if made using seawater ice, could achieve densities greater than freshwater and samples 1 through 4 could achieve densities greater than seawater.

Table 4.3: Maximum ice core densities from 12 samples collected on the north side ice wall at the Kennetcook River bridge in Winter 2012

Sample number	Date collected	Core mass ($\pm 1e^{-5}$kg)	Mass % sediment	Max freshwater ice density (kg/m^3)	Max seawater ice density (kg/m^3)
1	February 2	0.85505	20.83 ± 0.42	**1061**	**1075**
2	February 2	1.44966	17.01 ± 0.23	**1031**	**1045**
3	February 2	2.66522	28.65 ± 0.14	**1128**	**1142**
4	February 2	2.07161	19.63 ± 0.17	**1052**	**1066**
5	February 10	1.50737	3.84 ± 0.21	940	954
6	February 10	0.89392	10.90 ± 0.37	987	**1001**
7	February 10	1.60589	3.26 ± 0.19	937	950
8	February 10	0.98551	1.90 ± 0.31	928	942
9	February 10	1.02763	2.51 ± 0.30	932	945
10	February 16	2.82958	5.50 ± 0.23	951	964
11	February 16	2.69405	4.28 ± 0.21	943	957
12	February 16	1.92712	5.72 ± 0.11	952	966

4.4 Environmental measurements

Air temperature (T) over the study period was compared graphically with channel cross-sectional area to gain insight into any relationships (Figure 4.4). The shape of the temperature curve was similar to the shape of the channel cross-sectional area curve. To determine the timing of the buildup of ice in the channel and the timing of ice wall collapse, a spline was applied to T.

When the spline of temperature became negative, sediment-laden ice began to form. The fitted temperature curve crossed from positive to negative on December 22, 2011 (Figure 4.4). The time delay between the temperature spline becoming negative and the start of the formation of the ice walls was 18 days. The timing of the onset of ice wall formation was determined by the measured decrease in channel cross-sectional area and also by observation: January 9, 2012, was the first field date when ice walls were visibly forming. Thus, the ice walls may have begun to form at an earlier date.

The growth of ice continues over the period when temperatures are both negative and decreasing over time (Figure 4.4). After the minimum in the temperature curve plus the time lag, the channel cross-sectional area increases toward its summer value. In 2012, the minimum temperature occurred 20 days before the minimum channel cross-sectional area. The channel began to increase in cross-sectional area, in particular following the two subsequent high spring tides (shown as the two vertical lines in the bottom panel of Figure 4.4). Two measurements of channel cross-sectional area were taken between the two spring highs, during the neap part of the cycle. It was found that there was little change to channel cross-sectional area, despite the increase in temperature during that period. Most of the ice that made up the ice walls disappeared around the time of spring tides.

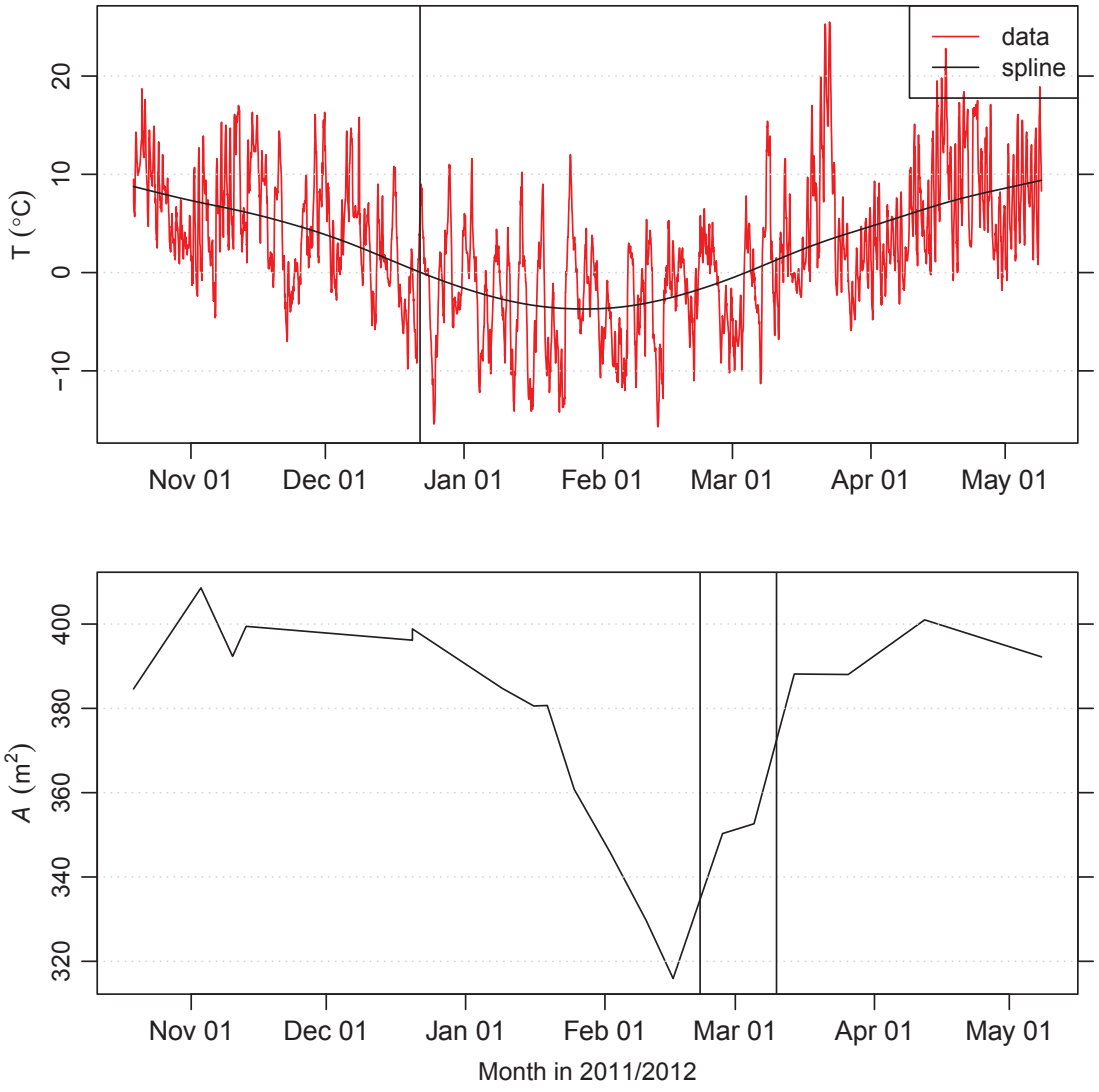

Figure 4.4: Top panel: air temperature (T) from October 19, 2011, to May 8, 2012, as well as a smoothed approximation. The vertical line represents the date when the temperature spline became negative. Bottom panel: channel cross-sectional area (A) over time. The two vertical lines represent the dates of the highest high tide over the spring-neap cycle that took place after the channel minimum cross-sectional area had been reached.

CHAPTER 5

DISCUSSION

The purpose of this study was to increase the understanding of the composition and processes of formation of large, sediment-laden ice blocks. This thesis addresses questions relating to how ice blocks form in the Minas Basin and what fraction of ice blocks may be neutrally or negatively buoyant. To explain the formation of ice walls in the narrow parts of channels connected to Minas Basin, two end-member hypotheses were developed. The first is Modified Bank Materials (MBM), in which the ice walls are caused by altered bank materials. The second is Modified Friction (MF), in which the ice walls are caused by altered channel flow energetics. This chapter discusses of the results presented in the previous chapter in the context of other studies.

5.1 Why do ice walls form?

The channel cross-sectional area, depth, and grain size data support the MF hypothesis (Figure 4.2). Ice walls form in the channels connected to the Minas Basin due to increased friction. Due to the presence of stranded ice (Figure 5.1), friction in the channel increases. Blocks of ice sit on the bed during a relatively large fraction of the tidal cycle. The stationary blocks cause turbulence and extract energy from the system. A visible, physical manifestation of this energy extraction from the flow is the cylindrical, sculpted form of stranded ice blocks (Figure 5.2). The increased friction causes the channel discharge to decrease. From the results of *Rinaldo et al.* (1999), the channel flow speed is assumed to be constant at equilibrium. When the discharge decreases, so does the flow speed. In order for equilibrium to be re-established at the decreased discharge, the channel cross-section must decrease.

The channel cross-sectional area decreased and the channel did not deepen, which would have been the case had the MBM hypothesis been correct. In the channel thalweg, the depth decreased from mid-December to mid-January (though, if the fall variability is included in the analysis, the change in depth between fall and the onset of winter is not significant). The evidence of shoaling, though limited, supports the MF hypothesis more than the MBM hypothesis, which predicted channel deepening. The channel depth increased at the onset of spring conditions, when the ice walls had fully collapsed (Figure 4.2). This result is in agreement with the MF hypothesis, which indicates that the channel velocity increases with the disappearance of the ice. The increased channel velocity causes erosion and an increase in the channel depth.

Figure 5.1: Stranded ice blocks at the Kennetcook River bridge. They may be swept away at high tide, but during much of the tidal cycle they add friction to the system.

Both MBM and MF hypotheses assume the channel will reach a wintertime equilibrium state. The channel cross-sectional area and the median grain size did not maintain a winter equilibrium over an extended period during winter 2012. There were fewer negative degree hours over winter 2012 than over the previous five winters (Table 5.1). In 2012, the ice walls may not have been fully formed, and may not have taken up as much of the channel cross-sectional area as they would over other winters. Also, median grain size may not have become constant at the winter equilibrium velocity because the velocity was adjusting to the changing state of the ice walls.

Figure 5.2: Stranded cake ice at Old Barns site. Due to friction (that occurs when blocks are stranded and when floating) the cakes have become roughly cylindrical.

The grain size results are in better agreement with the MF hypothesis than with the MBM hypothesis (Figure 4.2). Median grain size decreased throughout the winter, over the period during which the ice walls were forming. Grain size did not increase once the ice walls had fully formed, but this may be due to the small period during which the ice walls were at their maximum extent. When the ice walls collapsed the median grain size decreased further, in accordance with increased drag present in the channel as the ice walls produced blocks, which add drag to the channel. Melting ice blocks could also be releasing fine sediment into the channel. Grain size increased in the latter half of March and the beginning of April, as would be expected with increasing channel speed. The median grain size follows the anticipated pattern from the onset of winter to the start of spring; however, there are large natural variations in grain size outside winter, as seen from the October 2011 and May 2012 values.

5.1.1 Fractional increase in drag coefficient

The exact increase in the drag coefficient can not be determined from this study; however, a relationship between the *summer* and *onset of winter* drag coefficients can be described. In the following, subscripts 1, 2, and 3 represent non-winter, onset of winter, and winter,

respectively. By equation 2.1, the outside winter channel discharge is given by

$$Q_1 = A_1 U_{eq}, \tag{5.1}$$

where the subscript eq represents the equilibrium maximum flow velocity. When ice blocks first appear, the channel discharge and velocity decrease, and the cross-sectional area remains the same ($A_1 = A_2$), giving

$$Q_2 = A_1 U_2. \tag{5.2}$$

After the system adjusts to the decreased discharge, which is assumed to remain constant until the spring melt ($Q_2 = Q_3$), the discharge becomes,

$$Q_2 = A_3 U_{eq}, \tag{5.3}$$

invoking the Rinaldo relation (Section 2.8), in which the maximum velocity is regained. Therefore, substituting equation 5.2 into equation 5.3 gives,

$$A_1 U_2 = A_3 U_{eq}, \tag{5.4}$$

or

$$\frac{U_2}{U_{eq}} = \frac{A_3}{A_1}. \tag{5.5}$$

By equation 2.2, which is the force balance equation for the channel, the bottom drag coefficient is equal to

$$k = \alpha U^{-2}, \tag{5.6}$$

where $\alpha = -gh'\partial\eta/\partial x$. Using the above equation, the ratio of bottom drag coefficients between the onset of winter (extra friction) and non-winter (no extra friction) is given by

$$\frac{k_2}{k_1} = \frac{\alpha_2}{\alpha_1}\left(\frac{U_2}{U_{eq}}\right)^{-2}. \tag{5.7}$$

Substituting equation 5.5 into equation 5.7, a relationship between the decrease in cross-sectional area and the required increase in the bottom drag coefficient can be determined:

$$\frac{k_2}{k_1} = \frac{\alpha_2}{\alpha_1}\left(\frac{A_1}{A_3}\right)^2. \tag{5.8}$$

If it is assumed that α is constant, then α_2/α_1 is 1. In 2012, the decrease in channel cross-sectional area was 21%, and A_1/A_3 was 1.27. Then, by equation 5.8, k_2/k_1 was 1.6.

The calculated increase in k can be compared to literature values for obstructions in channels. *Hygelund and Manga* (2003) examined how the channel obstruction drag coefficient changed with the fraction of channel cross-sectional area that was obstructed by submerged logs. Though the logs in their study were suspended in mid-flow, away from the surface or bed, as compared to ice blocks, which strand on the bed, and the logs do not have the same shape as ice blocks, the increased friction they cause by partially obstructing a channel makes them effective for comparisons with the increased drag due to the ice. Separating the drag into two terms, the bottom drag and the friction caused by the obstructions, the force balance equation of *Hygelund and Manga* (2003) becomes:

$$-g\frac{\partial \eta(t)}{\partial x} = (k_b + k_{app}\frac{b}{2C})\frac{|u(t)|u(t)}{h'}, \tag{5.9}$$

where k_b is the bed drag coefficient, k_{app} is the obstruction drag coefficient (large woody debris), b is the diameter of the logs, and C is the distance between the logs.

For comparison with the present study, the channel bottom drag coefficient outside winter is given by k_1, and the bottom drag coefficient at the onset of winter is given by

$$k_2 = k_b + k_{app}\frac{b}{2C}, \tag{5.10}$$

where, in this case, k_{app} is due to the ice, and b is the diameter of the obstructing ice blocks and C is the distance between the blocks. The ratio of onset of winter to summer friction is

$$\frac{k_2}{k_1} = \frac{k_b + k_{app}\frac{b}{2C}}{k_1}. \tag{5.11}$$

It is assumed that $k_b \approx k_1$, meaning the bottom drag with the seabed changed little between outside winter and the onset of winter. Solving for C, the equation for the distance between

stranded ice blocks is

$$C = \frac{b}{2k_1} k_{app} \left(\frac{1}{k_2/k_1 - 1} \right). \tag{5.12}$$

Summer friction is assumed to be 2.5x10^{-3} (*Campbell et al.*, 1998) and k_{app} to be 0.36 (*Bathurst*, 1996), which is the drag coefficient of individual boulders on a riverbed. Using an ice block diameter (b) of 1 m, and since k_2/k_1 is 1.6, the distance between ice blocks (C) required to affect the change in channel cross-sectional area seen in the Kennetcook River is approximately 120 m.

This estimate means that relatively few stranded ice blocks are required within a tidal channel to effect the required change in drag. A possible reason for a large value of C is that ice blocks present large, blunt surfaces and thus produce drag over a large region, so few of them are necessary to increase the channel drag. Also, a stranded ice block spacing of 120 m may be a good estimate for tidal channels in the Minas Basin, since ice block distribution is not uniform within channels. Ice blocks only strand on parts of tidal channels that are left bare during portions of the tidal cycle. This means that in some areas, such as on bars (Figure 5.2), there can be a higher density of blocks than C requires, but in other parts of a channel, few blocks may be found. Blocks are also unlikely to remain stranded over more than a few tidal cycles, and while not stranded they contribute less drag to the system.

5.2 Environmental conditions that lead to ice walls and their collapse

Temperature was found to be a predictor of the timing of ice wall formation and collapse because it covaries with channel cross-sectional area, but leads the changes in cross-sectional area in time (Figure 4.4). The timing of the ice retreat is particularly important because it is when the ice walls became unstable and collapsed that the largest number of ice blocks were released into the water column. It was found that the timing of ice wall collapse depends on temperature in conjunction with the timing of spring tides.

The time difference between the temperature spline minimum and the collapse of the ice walls (or the time when the temperature spline becomes negative and the formation of ice walls) occurs because the channel takes time to adjust to a new temperature state. In other words, it took a number of days of near-continuous negative temperatures for the ice walls to begin to form and a number of days with positive daytime temperatures for

the ice walls to begin to collapse. In 2012, the time delay was 18 days for the start of the formation of the ice walls and 20 days for the start of the deterioration of the ice walls. There is some uncertainty in these lags due to the period between channel cross-sectional area measurements. Time between measurements was typically a week or more, which means the changes in channel morphology reported for specific times may have occurred at an earlier date, but were not recorded until the measurements were made.

The timing of ice wall deterioration also depends on the timing of spring tides subsequent to the temperature minimum. *Sanders* (2011) observed the total removal of ice fields from the banks of the Shubenacadie River with spring tides. The retreat of the ice walls in the Kennetcook River in 2012 happened in two stages. Following the time lag and the first spring tide, a significant amount of the ice was gone. After the second spring tide the channel returned to its summer cross-sectional area (the vertical lines in Figure 4.4 show the times of the highest spring tides). During neap tide, the channel cross-sectional area did not change significantly. Since the spring-neap cycle's period is two weeks, the timing of ice walls collapse could vary from year-to-year by up to fourteen days.

The timing of ice wall collapse for future years can be constrained based on the results reported here. It took two spring tides after the temperature spline reached its minimum to cause the ice walls to fully collapse. Since there are two weeks between subsequent spring tides, the minimum time of ice wall collapse is 14 days. The maximum, which would occur if the spring tide coincided with the temperature spline minimum, but that the water temperatures were not yet high enough to cause ice wall collapse, would be 28 days, since there would be two weeks before the first spring tide caused the start of the deterioration of the ice walls.

5.2.1 Was 2012 a typical year?

To compare the conditions for ice formation from winter 2012, with those of previous winters, the monthly cumulative negative degree hours for January, February, and March were calculated for the five years previous to 2012. Cumulative negative degree hours were calculated as a running sum of the magnitude of negative hourly temperatures over time. There were fewer negative degree hours in winter 2012 than in four of the previous five years (Table 5.1). The amount of ice and the state of the ice (unconsolidated or solid) are affected by the cumulative time that atmospheric temperatures are negative. The short period over which the ice walls were at their maximum extent and the unconsolidated

nature of the ice walls, during winter 2012, were likely not typical.

Table 5.1: Cumulative negative degree hours from January to March for the 5 years preceding 2012

Year	Cumulative negative degree hours (°C hr)			
	January	February	March	Total
2007	4311	4787	2142	11240
2008	3366	2937	2199	8502
2009	5773	2868	1998	10639
2010	2933	2147	807	5887
2011	3438	3344	1603	8385
2012	3056	2590	941	6587

Estimates were made of the start dates of ice wall formation and decay for the five years prior to 2012 (Table 5.2). Using the dates when the spline of temperature went from positive to negative and the time delay from 2012, the start dates of ice wall formation were estimated. Using the dates of temperature minima and the time delay from 2012, the start dates of ice wall deterioration were estimated. The timing of the start of ice wall formation over the six years examined varied by up to 31 days, whereas the timing of the start of ice wall collapse varied by only 16 days. Also, the number of negative degree hours over the winter did not necessarily indicate the length of time over which there would be ice walls. Neither of the two years with the greatest total degree hours, 2007 and 2009, had the longest period between the date of ice formation and ice decay. This suggests that colder winters do not necessarily lead to longer-lived ice walls. The ice walls, however, may reach their winter equilibrium states more quickly if the formation of ice was accelerated due to colder temperatures.

Table 5.2: Estimates of timing of ice wall formation and collapse in previous years

Year	Date of T transition: positive to negative	Probable start date of ice wall formation	Date of temperature minimum	Probable start date of ice wall collapse
2006-2007	2006-12-26	2007-01-13	2007-02-06	2007-02-26
2007-2008	2007-11-26	2007-12-14	2008-01-31	2008-02-20
2008-2009	2008-12-09	2008-12-27	2009-01-21	2009-02-10
2009-2010	2009-12-10	2009-12-28	2010-01-24	2010-02-13
2010-2011	2010-12-21	2011-01-08	2011-02-01	2011-02-21
2011-2012	2011-12-22	2012-01-09	2012-01-27	2012-02-16

5.3 Negatively buoyant ice

The four ice blocks that were negatively buoyant were all collected during the month of March, when above-zero temperatures are frequent. The blocks may have experienced differential release and/or fracturing prior to sampling, which increased their densities.

Negatively buoyant ice blocks may have been released into the Minas Basin once the spring melt began. Ice densities at that time were relatively high, and spring tides caused the ice walls to break away from the banks. A spring tide in late February removed a significant portion of the ice walls of the Kennetcook River. The subsequent spring high tide dislodged nearly all the remaining ice. The destruction of the ice walls caused a large input of ice blocks into the water column.

Due to the the sampling methods employed, the fraction of negatively buoyant ice blocks may not be representative of the ice blocks in the Minas Basin. Samples were collected from the outer layers of ice blocks, and since ice blocks are generally heterogenous, the samples may not be representative of the entire blocks. Also, only blocks with considerable sediment content were sampled, which may mean the fraction of negatively buoyant ice was smaller across the Minas Basin than found in this study's samples.

Despite the tendency for ice to become denser over the winter, the ice cores collected on February 2, 2012 had fractions of sediment that were higher than those collected on February 10 and 16. The average maximum density from the four cores taken on February 2 was 1289.9 $\pm$0.8 kg/m^3. The percent difference between the core average maximum density from February 2 and from February 10 and February 16 are 25.9$\%$ and 24.7$\%$, respectively. The differences can be accounted for by examining the environmental conditions around the time that the cores were drilled (Figure 3.4). The conditions were similar on the three days prior to and on the days of ice core collection. Maximum daily temperatures were a mix of above and below zero, there was little precipitation, and windspeeds were low. The height of the tides is what differentiates these three periods. A neap tide occurred on February 2, and for approximately 4 days leading up to that date, the tides were lower than they were on February 10 and February 16. February 10 was very close to a spring tide and February 16 was close to a high tidal-range neap tide. It is possible that the top of the ice banks were not exposed to water, so no ice was deposited on their top surface during the four days leading up to February 2. Also, on January 29 and 30, temperatures went above zero during the day. Above zero temperatures may have

caused differential release that increased the density of the ice. It is also possible that the sun provided radiation energy during the days leading up to February 2, which could cause further differential release of the ice. The inundation of the high tides on the two later dates may also have effected the sediment-to-water ratio. If bubbles in the ice are filled with water, then though the ice would be denser, the ratio of sediment-to-water would be lower. If the air volume were known it would be possible to determined whether the ice had indeed become more dense over time, as expected.

Of the 12 ice cores drilled from the ice walls along the Kennetcook River, assuming the ice contained no air, 4 had densities greater than freshwater and seawater. Air volume of the ice cores was not measured. The volume of the ice core cylinder was known, but when the ice was cored it was found that there were hollow sections in the ice walls that could not easily be measured. The ice walls in 2012 were also porous and often in a state of partial melting, rather than solid. Winter 2012 was warmer than the five previous years (Table 5.1). As a result, the ice cores collected were unconsolidated masses of ice and the core volumes were unmeasurable.

Even solid ice blocks can contain air pockets. *Sweet* (1968) noted that when drilling into a large, solid, stranded ice block in the Salmon River Estuary, the interior of the block contained an air pocket of up to about a meter in length and about 30 cm in width. Though the air content of the ice cores was not determined in this study, ice core maximum densities were greater than what is required for negative buoyancy. Ice walls can produce blocks with high enough densities to be negatively buoyant while at the same time containing a volume of air. If the ratio of sediment to ice in the ice walls increased later in the season, an even higher fraction of the volume of the ice could be made up of air and the ice would still be negatively buoyant, but one, with a sediment mass percentage of over 28%, was close.

Table 5.3 summarizes studied that reported either sediment mass fractions or sediment volume fractions. Sediment mass percentages were determined from sediment mass per volume of ice reported by *Hind* (1875) and *Sanders* (2011). Sediment mass percentages were calculated using the densities of freshwater ice and quartz. The assumed densities add uncertainty to the sediment mass percentage for these two studies that does not exist for the others. Fortunately, the studies that involved the collection of the largest number of samples also measured and reported sediment mass fractions (*Sweet*, 1968; *Knight and*

Dalrymple, 1976).

The sediment mass fractions in Table 5.3 allow for an estimate of qualitative buoyancy, however, they do not take the ice air content into account. For example, *Sweet* (1968) analyzed three samples of sediment-laden ice from the Minas Basin (one from the Salmon River Estuary and two from the mudflats near Highland Village, which is approximately 10 km west of Debert Beach) and found densities of 870.8, 599.1, and 730.4 kg/m^3. One of the samples analyzed by Sweet contained 18.06% sediment, which should make the sample negatively buoyant, however, the density of that block was only 870.8 kg/m^3. Since sediment and ice each individually have densities greater than those of Sweet's samples, air must account for part of the volume.

Most of the sediment-laden ice formed in the Minas Basin likely has a relatively high air volume fraction. Ice blocks formed in ice fields and ice walls are often composite ice blocks, made up of many blocks haphazardly frozen together, which can cause large air pockets to form. Five of 13 ice block sampled in 2012 had sediment mass fractions greater than 16%, but only those 2 with sediment mass percentages of 31.0 and 37.5 were found to have densities greater than seawater. The minimum sediment mass fraction required for neutral buoyancy of sediment-laden ice containing air in freshwater was 31%. Using this result, none of the ice cores collected (Table 4.3) contained the required sediment mass fraction to cause them to be neutrally buoyant.

Using the minimum sediment mass fraction required for neutral buoyancy, the volume of air in neutrally buoyant ice blocks can be estimated. Assuming the air adds no mass to the ice blocks, the equation for the ratio of the air volume (V_a) and the total volume is given by

$$\frac{V_a}{V_t} = \frac{1}{V_t}(V_t - V_i - V_s), \tag{5.13}$$

and substituting for masses and densities, becomes

$$\frac{V_a}{V_t} = \frac{\rho}{M_t}(\frac{M_t}{\rho} - \frac{M_i}{\rho_i} - \frac{M_s}{\rho_s}). \tag{5.14}$$

If freshwater ice and seawater are assumed for the densities of the ice and water, then the estimate of the volume percentage of trapped air in neutrally buoyant ice blocks is 11%.

In sampling experiments, such as the drilling of ice cores in this study and those listed in Table 5.3, (with the exception of *Sweet* (1968)), it is not possible to know the air volume

fraction of the ice samples. Maximum densities may be calculated, but it is the density of the ice blocks, including air, that is required to fully determine their buoyancy.

Table 5.3: Summary of sediment mass percentages in samples from previous studies

Study	Date collected	Site	Sample	Sediment mass %	Probable buoyancy
Hind (1875)	Unknown	Avon River	1	0.8	positive
			2	0.3	positive
Bancroft (1905)	Unknown	Cornwallis River	Unknown (15.4kg)	3.2	positive
Sweet (1968)	March 21, 1968	Salmon River Estuary	1	18.06	positive
		North shore of Cobequid Bay	2	1.27	positive
			3	3.05	positive
Knight and Dalrymple (1976)	Last week in February, 1973 and/or 1974	South shore of Cobequid Bay	1	4.98	positive
			2	13.84	positive
			3	21.98	negative
			4	0.07	positive
			5	0.08	positive
			6	0.17	positive
			7	1.26	positive
			8	0.78	positive
			9	0.59	positive
			10	0.60	positive
			11	0.81	positive
			12	1.73	positive
			13	0.73	positive
			14	5.97	positive
			15	3.64	positive
			16	0.07	positive
			17	15.71	positive
			18	22.23	negative
			19	1.11	positive
			20	0.85	positive
			21	0.65	positive
			22	0.78	positive
Sanders (2011)	March 26, 2009	Avon River	1	19.1	negative

5.4 Do negatively buoyant ice blocks pose a threat?

On an exceptionally high spring tide, particularly in the melting season, a large portion of the ice blocks can be swept out of tidal channels and into the Minas Basin with the ebb tide. Ice blocks form that are negatively buoyant. Ice blocks also form that are close to neutrally buoyant. In the turbulent water of the Basin, neutrally buoyant blocks could easily be swept to any depth in the water column. These blocks exist and they could pose a threat to bottom-anchored man-made structures if they remain intact throughout a journey across the Minas Basin. It is beyond the scope of this project, however, to predict how the ice blocks behave once they are in the open Basin and headed in the direction of the Minas Passage.

CHAPTER 6

CONCLUSIONS

6.1 Conclusions

The goal of this research was to increase the understanding of the composition and the processes of formation of large, sediment-laden ice blocks in the Minas Basin. The aim was to understand how ice blocks form and what fraction may have densities that make them neutrally or negatively buoyant. Since large ice blocks are produced from ice walls that form in tidal channels, this study focused on understanding ice bank processes and properties of tidal channels. The conclusions of this thesis are:

1. The fraction of ice blocks collected from the Minas Basin that were negatively buoyant in freshwater was 10% (Section 4.3), which is roughly consistent with previous estimates. Four of twelve ice cores collected from the ice cliffs along the Kennetcook River contained enough sediment to become denser than seawater. Through plucking and differential release, sediment-laden ice increases in density over the winter and is most likely to become negatively buoyant as the spring melt approaches.

2. Channels change their morphology from summer to winter due to altered channel flow energetics, following the Modified Friction hypothesis (Section 2.8). Ice cliffs form when anchored ice obstructs tidal channels, increasing drag and decreasing flow speed. In 2012, the formation of ice walls caused the cross-sectional area of the Kennetcook River to decrease by 21%.

3. Air temperature data analysis improved the understanding of the timing of ice wall formation and collapse. Air temperature covaried with the channel cross-sectional

area, plus a time lag (Section 4.4). Large ice blocks separated from the walls during the two spring tides following a 20-day time lag of the minimum air temperature (Section 5.2). The ice walls began to form 18 days after the temperature spline became negative.

4. Air-free freshwater ice was calculated to require a sediment mass fraction of 16% to be neutrally buoyant in seawater (Section 3.3). From ice block samples, a minimum of 31% of the mass of ice blocks containing air was required for ice to be negatively buoyant in freshwater (Section 5.3). An estimate of the volume of trapped air in a neutrally buoyant ice block with 31% sediment by mass is 11% (Section 5.3).

6.2 Future research

1. The time lags may vary between years. If the range of the lags were known, then the timing of ice wall formation and deterioration could be better predicted. The ice walls retreat on the spring tides after the temperature begins to increase. A suggested hypothesis is that ice walls will collapse after the first two spring tides following the increase in temperature. The time lag should depend on the time between the temperature minimum and the subsequent spring tides, which means the lag could vary from year-to-year by up to two weeks; from 14 days to 28 days.

2. An experimentally-measured drag coefficient for ice present in a tidal channel would allow for a more precise estimate of the extent of the ice walls. The drag coefficient for ice could be developed as a function of the fraction of channel cross-sectional area obstructed by ice and as a function of the relative proximity of stranded ice blocks. The friction term due to ice in the force balance equation for the channel would be similar to that of *Hygelund and Manga* (2003) for large woody debris (Section 5.1).

3. This study examined the timing of release of sediment-laden ice blocks from the ice walls, but did not include what became of the ice blocks once they had shed from the ice walls. If the trajectories of the ice blocks were monitored, then their threat to bottom-anchored tidal energy generators could be better understood.

APPENDIX A

Table A.1: Kennetcook River depth, referenced to the high water mark (section 3.1), at 41 positions across the channel width (Dist.), from October 19, 2011 to May 8, 2012. All measurements in metres.

Dist.	10-19	11-03	11-10	11-13	12-20	12-20	01-09	01-16	01-19	01-25	02-02	02-10	02-16	02-27	03-05	03-14	03-26	04-12	05-08
0	-1.25	-1.15	-1.25	-1.2	-1.18	-1.2	-1.24	-1.26	-1.24	-1.24	-1.45	-1.32	-1.37	-1.18	-1.27	-1.15	-1.19	-1.11	-1.17
2.45	-0.92	-0.37	-0.51	-0.49	-0.49	-0.48	-0.52	-0.54	-0.51	-0.51	-0.66	-0.81	-0.64	-0.5	-0.5	-0.46	-0.46	-0.4	-0.47
4.8	0.03	0.02	0.01	0.05	-0.16	0.05	0.03	0.04	0.02	0.03	0.00	0.11	0.11	0.06	0.08	0.12	0.15	0.23	0.14
7.15	0.34	0.32	0.33	0.34	0.03	0.36	0.31	0.30	0.31	0.34	0.28	0.33	0.33	0.29	0.29	0.37	0.42	0.46	0.35
9.55	0.40	0.39	0.39	0.41	0.35	0.43	0.38	0.37	0.38	0.40	0.35	0.40	0.35	0.39	0.37	0.48	0.53	0.48	0.46
11.9	1.57	1.56	1.55	1.55	1.65	1.58	1.60	1.58	1.59	1.28	1.35	0.90	1.11	1.17	1.39	1.63	1.47	1.63	1.46
14.3	2.21	2.20	2.06	2.12	2.12	2.14	2.2	1.99	2.00	1.50	1.47	0.91	0.93	1.04	0.98	2.19	2.07	2.06	2.07
16.7	5.46	5.52	3.36	3.48	3.41	3.52	3.46	2.59	3.09	1.37	1.92	0.43	0.56	2.45	2.65	3.37	3.39	3.39	3.34
19.05	4.56	4.43	4.05	4.65	4.38	4.28	4.46	3.70	3.81	3.00	2.8	0.76	1.11	3.53	3.23	4.44	4.20	4.67	4.44
21.4	5.76	5.25	5.05	5.86	5.39	5.42	5.7	5.17	5.13	4.41	3.2	3.32	6.41	5.56	5.18	6.09	5.76	6.3	5.81
23.8	6.28	6.06	6.28	6.18	6.43	6.26	6.55	5.26	6.35	6.24	6.09	5.87	6.49	6.29	6.24	6.60	6.68	6.38	6.54
26.15	7.02	6.84	7.02	7.28	7.02	7.27	6.98	5.45	6.98	6.84	6.82	6.99	6.48	6.81	7.18	7.65	7.03	7.67	7.25
28.5	7.49	7.48	7.48	7.49	7.51	7.43	7.28	7.58	7.49	7.28	7.07	7.19	7.02	7.32	7.42	7.58	7.78	7.71	7.43
30.9	7.28	7.32	7.42	7.44	7.32	7.03	7.08	7.36	7.07	7.14	7.07	7.20	7.19	7.21	7.15	7.57	7.72	7.87	7.63
33.27	7.09	7.22	7.31	7.25	7.28	7.2	6.99	7.14	7.27	7.32	7.08	7.37	7.11	7.15	6.95	7.45	7.39	7.41	7.36
35.66	6.74	7.08	7.16	7.29	7.15	7.1	6.77	7.1	7.12	7.19	6.92	7.01	7.32	7.26	6.64	7.38	7.17	7.11	7.15

Continued on next page

Table A.1 – *Continued from previous page*

Dist.	10-19	11-03	11-10	11-13	12-20	12-20	01-09	01-16	01-19	01-25	02-02	02-10	02-16	02-27	03-05	03-14	03-26	04-12	05-08
37.96	6.70	7.16	7.25	7.38	7.12	7.20	6.73	6.94	7.02	7.07	6.74	6.99	6.76	6.86	6.75	7.30	7.12	7.17	7.28
40.4	7.30	7.55	7.64	7.64	7.49	7.46	7.24	7.46	7.43	7.24	7.43	7.7	7.42	7.93	7.51	8.19	7.52	7.42	7.70
42.8	7.62	7.99	7.86	7.64	7.88	7.67	7.58	7.78	7.82	7.67	7.85	7.5	7.77	8.15	7.72	7.72	8.13	7.92	7.95
45.15	5.43	4.57	5.57	5.38	5.46	5.57	5.43	4.86	5.06	5.52	4.08	7.41	4.82	5.63	7.67	5.72	5.73	5.45	5.49
47.52	5.76	5.69	5.61	5.74	5.72	5.65	5.75	5.02	5.73	5.79	4.51	3.76	5.28	5.62	5.78	5.71	5.74	5.79	5.70
49.7	7.41	7.54	5.70	5.75	5.64	7.41	5.49	4.98	5.69	7.35	5.25	5.28	5.42	5.67	5.66	5.76	5.68	7.32	5.74
52.25	7.77	7.72	7.71	7.79	7.80	7.64	7.77	7.77	7.62	7.55	7.61	7.50	7.59	7.67	7.49	7.51	7.97	7.78	7.82
54.65	7.65	7.59	7.70	7.57	7.58	7.60	7.56	7.53	7.52	7.48	7.58	7.63	7.5	7.43	7.47	7.66	7.78	7.39	7.71
57.03	7.17	7.36	7.24	7.29	7.32	7.31	7.18	7.35	7.19	7.22	6.94	7.69	7.09	6.74	6.95	7.39	7.32	7.36	7.4
59.39	7.09	7.41	7.35	7.54	7.4	7.47	7.38	7.31	7.00	6.99	6.51	7.10	6.71	6.13	6.41	7.25	7.31	7.45	7.33
61.78	6.60	7.74	7.39	7.52	7.34	7.32	6.94	7.03	6.67	6.48	6.00	6.11	5.66	5.74	5.51	6.79	6.84	7.26	7.13
64.16	5.64	7.53	7.02	7.04	7.13	7.18	6.80	6.52	6.35	6.12	5.54	2.80	4.51	5.55	5.81	6.32	6.79	6.92	6.85
66.53	4.98	7.07	6.97	6.77	7.00	6.98	6.34	6.20	5.98	5.71	4.79	3.95	1.50	4.87	4.55	5.84	6.00	6.52	6.31
68.9	4.54	6.56	6.35	7.06	6.60	6.61	5.72	5.86	5.59	5.11	4.95	4.10	1.40	3.58	3.51	5.38	5.26	5.93	5.14
71.28	4.25	5.59	5.41	6.06	5.90	6.05	4.92	5.60	5.32	4.84	4.64	2.76	1.28	3.46	3.35	4.81	4.19	5.15	4.87
73.67	4.01	4.71	4.57	4.52	4.9	4.83	4.52	4.94	4.56	3.53	4.33	1.77	1.67	3.22	3.26	3.27	3.73	4.03	4.3
76.05	3.08	3.25	3.31	3.27	3.27	3.33	3.21	3.44	3.33	2.07	2.53	1.19	0.73	1.19	2.00	2.83	3.09	3.16	3.33
78.43	1.93	2.06	2.25	2.09	2.04	2.01	2.2	4.14	2.10	0.70	0.71	0.56	0.49	1.10	0.70	2.18	1.99	2.23	2.29
80.79	0.42	0.47	0.51	0.56	0.50	0.44	0.62	1.14	0.63	0.46	0.33	0.42	0.48	0.55	-0.41	0.61	0.51	0.68	0.81
83.17	-0.51	-0.49	-0.46	-0.48	-0.48	-0.52	-0.55	-0.41	-0.51	-0.56	-0.55	-0.45	-0.5	-0.47	-0.93	-0.45	-0.46	-0.41	-0.38
85.55	-1.03	-1.01	-0.98	-0.96	-1.03	-1.02	-1.01	-0.97	-1.03	-1.01	-1.03	-0.98	-1.04	-1.04	-1.18	-0.95	-0.95	-0.95	-0.96
87.94	-1.20	-1.23	-1.20	-1.16	-1.19	-1.24	-1.22	-1.17	-1.19	-1.20	-1.22	-1.25	-1.20	-1.21	-1.55	-1.13	-1.10	-1.08	-1.10
90.3	-1.59	-1.57	-1.57	-1.02	-1.61	-1.57	-1.60	-1.59	-1.58	-1.52	-1.70	-1.70	-1.60	-1.56	-2.05	-1.69	-1.51	-1.45	-1.49
92.66	-2.95	-2.98	-2.91	-2.96	-2.96	-2.97	-2.95	-2.96	-2.94	-3.00	-3.01	-2.96	-3.02	-2.97	-2.97	-2.95	-2.94	-2.78	-2.89
95.05	-3.47	-3.50	-3.47	-3.47	-3.48	-3.48	-3.49	-3.46	-3.49	-3.50	-3.51	-3.51	-3.60	-3.51	-3.50	-3.48	-3.48	-3.48	-3.45

BIBLIOGRAPHY

Anderson, R. J., B. P. Bledsoe, and W. C. Hession, Width of streams and rivers in response to vegetation, bank material, and other factors, *Journal of the American Water Resources Association*, pp. 1159–1172, 2004.

Bancroft, J. A., Ice-borne sediments in Minas Basin, NS, *The McAlpine Publishing Co. Ltd.*, 1905.

Bathurst, J. C., Field measurement of boulder flow drag, *Journal of Hydraulic Engineering*, *122*, 167–169, 1996.

Campbell, A., J. Simpson, and G. Allen, The dynamical balance of flow in the Menai Strait, *Estuarine, Coastal and Shelf Science*, *46*, 449–455, 1998.

Carver, R., *Procedures in sedimentary petrology*, John Wiley & Sons Incorporated, 1971.

Cornett, A., J. Cousineau, and I. Nistor, Hydrodynamic impacts due to tidal power lagoons in the upper Bay of Fundy, Canada, *Technical report*, National Research Council Canada, 2011.

Cox, M. G., and P. M. Harris, Software support for metrology best practice guide no. 6: Uncertainty evaluation, *Tech. rep.*, National Physical Laboratory, 2006.

Desplanque, C., Ice conditions in tidal rivers and estuaries, *Tech. rep.*, Canada Department of Forestry and Rural Development, Rural Development Branch Atlantic Region, 1967.

Desplanque, C., and D. I. Bray, Winter ice regime in the tidal estuaries of the northeastern portion of the Bay of Fundy, New Brunswick, *Canadian Journal of Civil Engineering*, *13*, 1986.

Desplanque, C., and D. J. Mossman, A review of ice and tide observations in the Bay of Fundy, *Atlantic Geology*, *34*, 195–209, 1998.

Desplanque, C., and D. J. Mossman, Tides and their seminal impact on the geology, geography, history, and socioeconomics of the Bay of Fundy, eastern Canada, *Atlantic Geology*, *40*, 2004.

Environment Canada, National climate data and information archive, 2013.

Garrett, C., and P. Cummins, The power potential of tidal currents in channels, *Proceedings of the Royal Society*, *461*, 2563–2572, 2005.

Gordon, D. C. J., and C. Desplanque, Ice dynamics in the Chignecto Bay region of the Bay of Fundy, *Proceedings of the Workshop on Ice Action on Shores, Rimouski, Québec*, pp. 35–52, 1981.

Gordon, D. C. J., and C. Desplanque, Dynamics and environmental effects of ice in the Cumberland Basin of the Bay of Fundy, *Canadian Journal of Fisheries and Aquatic Sciences*, *40*, 1331–1342, 1983.

Gran, K., and C. Paola, Riparian vegetation controls on braided stream dynamics, *Water Resources Research*, *37*, 3275–3283, 2001.

Haynes, W. M. (Ed.), *CRC Handbook of Chemistry and Physics*, 92 ed., Taylor and Francis Group, 2012.

Hickin, E. J., Vegetation and river channel dynamics, *Canadian Geographer*, pp. 11–126, 1984.

Hind, H. Y., The ice phenomena and the tides of the Bay of Fundy, *Canadian Monthy and National Review*, *8*, 1875.

Hygelund, B., and M. Manga, Field measurements of drag coefficients for model large woody debris, *Geomorphology*, *51*, 175–185, 2003.

Istanbulluoglu, E., R. Bras, H. Flores-Cervantes, and G. Tucker, Implications of bank failures and fluvial erosion for gully development: Field observations and modeling, *Journal of Geophysical Research*, *110*, 2005.

Knight, R., and R. Dalrymple, Winter conditions in a macrotidal environment, Cobequid Bay, Nova Scotia, *Revue de géographie de Montréal*, *30*, 65–85, 1976.

Leopold, L., M. Wolman, and J. Miller, *Fluvial Processes in Geomorphology*, Dover Publications, 1995.

Leopold, L. B., and T. Maddock, The hydraulic geometry of stream channels and some physiographic implicationns, *Geological Survey Professional Paper 252*, 1954.

Ollerhead, J., D. van Proosdij, and R. G. D. Davidson-Arnott, Ice as a mechanism for contributing sediments to the surface of a macro-tidal saltmarsh, Bay of Fundy, *Canadian Coastal Conference*, pp. 345–358, 1999.

Rinaldo, A., S. Fagherazzi, S. Lanzoni, M. Marani, and W. Dietrich, Tidal networks 3. landscape-forming discharges and studies in empirical geomorphic relationships, *Water Resources Research*, *35*, 3919–3929, 1999.

Sanders, R. E., Marine ice and other issues during harvest of tidal electricity from Nova Scotia's Minas Passage in 2011, *Journal of Ocean Technology*, *6*, 33–55, 2011.

Sanders, R. E., and E. Baddour, Documenting ice in the Bay of Fundy Canada, *Tech. rep.*, National Research Council Canada, Institute for Ocean Technology, 2006.

Sanders, R. E., C. Byers, and E. Baddour, Tidal power and migratory sub-surface ice in the Bay of Fundy, Canada, in *The Proceedings of the 2007 International Conference On Offshore Mechanics and Arctic Engineering*, pp. 1–36, The Fundy Tidal Energy

Technical Advisory Group and The Ocean Energy Environmental Research Association, 2008.

Schumm, S., The effect of sediment type on the shape and stratification of some modern fluvial deposits, *American Journal of Science*, *258*, 177–184, 1960.

Sweet, C. E., Report on ice conditions in Minas Basin and Chignecto Bay, and their embranchments for January - March, 1968, *Tech. rep.*, Atlantic Tidal Power Programming Board, 1968.

Taylor, J. R., *An introduction to error analysis: the study of uncertainties in physical measurements*, University Science Books, 1997.

Timco, G. W., and R. M. W. Frederking, A review of sea ice density, *Cold Regions Science and Technology*, *24*, 1–6, 1996.

vanProosdij, D., J. Ollerhead, and R. G. D. Davidson-Arnott, Seasonal and annual variations in the volumetric sediment balance of a macro-tidal salt marsh, *Marine Geology*, *225*, 103–127, 2006.

Wiberg, P., and J. Smith, Calculations of the critical shear stress for motion of uniform and heterogeneous sediments, *Water Resources Research*, *23*, 1471–1480, 1987.